MATERIALS TECHNOLOGY FOR COAL-CONVERSION PROCESSES
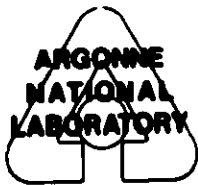
Progress Report for July—September 1980

ARGONNE NATIONAL LABORATORY, ARGONNE, ILLINOIS

TABLE OF CONTENTS

LIST OF FIGURES

LIST OF TABLES

MATERIALS TECHNOLOGY FOR COAL-CONVERSION PROCESSES
Progress Report for
July-September 1980

HIGHLIGHTS

Task A -- Evaluation of Ceramic Refractories for Slagging Gasifiers
         (C.R. Kennedy, R.J. Fousek, and S.W. Kreis)

     Analysis of a failed mullite refractory lining in the Grand Forks
Energy Technology Center slagging gasifier revealed that the mullite had
reacted with sodium hydroxide to form carnegieite and beta-alumina. This
reaction is accompanied by a substantial volume change, with resultant failure
by chemical spalling.

     Analysis of the corrosion of refractories in test run 12 is con-
tinuing and will be presented in the next quarterly report.

Task B -- Development and Application of Nondestructive Evaluation Methods
         for Coal-conversion Processes (W.A. Ellingson, C.A. Youngdahl,
         D.S. Kupperman, M.J. Caines and N.F. Fiore)

     Work continued on the high-temperature ultrasonic erosion scanner.
Activities included development of pressure-coupling methods (to augment the
stud welding method already developed), new field installations on tar separator
cyclones at Morgantown Energy Technology Center (METC), and extensive prepar-
ations for a new field installation on the Exxon Donor Solvent Plant at Baytown,
TX.

     Flaw characterization studies were initiated this month as part of
a study on a flawed section of 4-in. Type 347 stainless steel piping from the
SRC plant in Ft. Lewis, WA. A hard "scale" on the inner surface caused initial
inspection problems. Extensive ultrasonic and metallographic study indicates
that the "flaw" detected in the pipe wall is a deep internal blister.

     A preliminary design was completed for a slurry flow loop for
acoustic leak detection studies. The facility will allow testing at tem-
peratures up to 500°C and pressures up to 1000 psi (6.9 MPa). Available flow
times will range from 15 to 60 s, depending on test section configuration.

Task C -- Corrosion Behavior of Materials in Coal-conversion Processes
         (K. Natesan)

     A number of tests have been conducted to examine the role of com-
bustion-gas stoichiometry on the corrosion behavior of materials for use
as air and steam heat-exchanger tubes. The alloys selected for the investigation
are carbon steel, Fe-2-1/4Cr-1Mo and Fe-9Cr-1Mo ferritic steels, Type 310
stainless steel, and Incoloy 800. Experiments are in progress with alloy
specimens that were coated with various deposits such as CaO and $CaSO_4$.

Task D -- Erosion Behavior of Materials in Coal-conversion Processes
(J.Y. Park)

Room-temperature erosion tests were performed on 1015 carbon steel, Type 304 stainless steel, Incoloy 800, Type 310 stainless steel, and Stellite 6B in the ANL low-temperature erosion test apparatus using 150-μm Al_2O_3 particles with an impact velocity of 22 m/s and impact angles of 16-81° in an air environment. The erosion rates calculated from weight loss are in the range of 0.01-0.08 mg/g, and are in good agreement with the rates obtained from the high-temperature erosion-corrosion test apparatus.

Task E -- Failure Analysis (D.R. Diercks and G.M. Dragel)

Four experimental thermowells have undergone a total of six runs in the U-Gas Pilot Plant and are presently being examined. Three additional thermowells have been installed in the plant for a similar series of exposures. The analysis of a cracked hot-gas sampler coupling from the HYGAS® Pilot Plant has been completed, and the failure has been found to result from excessive sulfidation of Inconel 182 weld metal and the adjacent RA 330 base metal. An analysis of a cracked product gas line section from the Bi-Gas pilot plant is presently being performed, and the possibility that failure was caused by caustic- or oxygen-assisted stress-corrosion cracking is being explored. A perforated product gas line expansion joint from the U-Gas Pilot Plant was found to have failed owing to chloride-induced pitting. The chlorides were introduced as an impurity present in the coal char and ash handled by the component, and intermittent wetting of the inner surface occurred because of condensation during shutdowns.

MATERIALS TECHNOLOGY FOR COAL-CONVERSION PROCESSES
Progress Report for
July–September 1980

FOR:WORD

This materials engineering program, begun in 1974, includes
studies on ceramic (refractory) and metallic materials presently
being used or intended for use in coal-conversion processes. The
program entails efforts in nondestructive testing and failure
analysis, as well as studies of erosive wear, corrosion, and refrac-
tory degradation. Appropriate laboratory and field experiments
are integrated such that the results have impact on present pilot-
and demonstration-plant and proposed full-scale designs. This
report, for the period July–September 1980, presents the technical
accomplishments of the program.

ABSTRACT

During the present reporting period, failure analysis of the re-
fractory lining of the Grand Forks Energy Technology Center slagging gasifier
revealed that sodium hydroxide had reacted with the refractory, causing a
large volume change and consequent spallation.

Laboratory studies on pressure coupling of acoustic waveguides to
pressure boundaries for long-term erosive wear measurements show that the use
of annealed copper foil [0.25–0.76 mm (10–30 mil) thick] with a contact
pressure of 50–70 MPa (7–10 ksi) can yield satisfactory coupling in the pre-
sence of thermal cycling. Pressure coupling will be used in a field instal-
lation at the Exxon Donor Solvent coal liquefaction pilot plant. Long [0.6-
and 1.2-m (2- and 4-ft.)] waveguides have been designed for extending high-
temperature erosion studies to preheater coils. These waveguides employ a
0.5% taper to prevent reinforcement of the acoustic waves reflecting off the
side walls, and side-wall texturing to reduce noise. Erosion scanning was
extended to the tar separator cyclones at Morgantown, WV. The scanner cur-
rently in operation at METC has shown good stability even after several
start-ups (thermal cycling). Flaws detected by ultrasonic methods included
a unique metallic blister which had formed on the inside of a 4-in. Type 347
stainless steel piping section at SRC.

High-temperature corrosion studies have been initiated to investi-
gate effects of deposits such as CaO and $CaSO_4$ on corrosion rates of
Fe-2-1/4Cr-1Mo and Fe-9Cr-1Mo ferritic steels.

Erosion studies at room temperature and atmospheric pressure were con-
ducted on 1015 carbon steel, 304 and 310 stainless steel, Incoloy 800, and
Stellite 6B. Impact particles were 150-μm Al_2O_3 with impact angles of 16–81°.
Weight-loss measurements are in good agreement with prior work.

Materials studies for instrumentation included studies of thermo-
wells at the U-Gas plant run by IGT. Six runs have now been completed using
the thermowells, with a total exposure time of 1200 h. Two failure analyses
were conducted during the present quarter. Analysis of a product gas line
from Bi-Gas indicates that failure was caused by caustic- or oxygen-assisted
stress-corrosion cracking. A product gas line expansion joint from U-Gas
was also examined; at present, chloride-induced pitting seems to have been
the cause of this failure, which was initiated at the inner surface.

INTRODUCTION

Economical, reliable, and safe conversion of coal into clean and
usable alternate fuels will be advanced through the use of durable materials
of construction. The technical information base applicable to the behavior
of materials in the operating environments characteristic of various coal-
conversion processes is extremely limited. Hence, reliable materials selection
and lifetime prediction are difficult to achieve. This program is designed to
provide part of the materials information necessary for successful operation
of coal-conversion systems. The present report is the twenty-second progress
report submitted by ANL to the Office of Advanced Research and Technology,
Office of Fossil Energy under Project Number 7106, "Materials Technology for
Coal-conversion Processes".

The project includes five tasks: (A) Evaluation of refractories
exposed to coal slag under conditions typical of those encountered in slagging
gasification processes; (B) development and application of nondestructive
evaluation methods; (C) evaluation of the corrosion behavior of commercial
alloys; (D) development of analytical models to predict the erosive-wear
behavior of materials; and (E) analyses of failed coal-conversion plant
components.

Task A -- Evaluation of Ceramic Refractories for Slagging Gasifiers
(C.R. Kennedy, R.J. Fousek, and S.W. Kreis)

The main effort during this quarter was devoted to the failure analysis of a mullite refractory lining from the Grand Forks Energy Technology Center (GFETC) gasifier. The analysis of the corrosion of the refractories from test run 12 is continuing and will be presented in the next quarterly report.

The Grand Forks Energy Technology Center operates a single-stage pressurized fixed-bed slagging gasifier. The upper three sections of this gasifier are lined with high-grade mullite tile backed by insulating firebrick and insulating castable refractory. The presence of molten slag is confined to a lower section of the gasifier.

The mullite refractory cracked and spalled after exposure to the coal-gasification atmosphere for a total of about 125 h at a hot-face temperature of $\sim$ 1000°C ± 150°C.[1] The pressure of the process was $\sim$ 25 bars (2.5 MPa). Most of the coal used during the exposure period was a high-sodium lignite from the Indianhead mine near Beulah, ND, with the nominal ash and slag compositions shown in Table I. The differences in composition indicate that Na and S have been volatilized extensively.

Samples of the refractory before and after exposure to the gasification atmosphere were received from GFETC. No records were available to identify the brand name or vendor. X-ray analysis using CaKα revealed that the as-received sample was composed mainly of mullite ($Al_6Si_2O_{13}$) with lesser amounts of free alumina (Al_2O_3) (Fig. 1). Scanning electron microscopy with energy dispersive x-ray analysis (SEM-EDX) revealed only Al and Si, as shown in Fig. 2. No sodium was detected.

X-ray analysis of the exposed specimen (Fig. 3) indicated that the mullite had been almost completely converted into carnegieite ($NaAlSiO_4$) and beta-alumina ($NaAl_{11}O_{17}$). Minor amounts of mullite, alumina, carbon, and NaOH were detected. The x-ray pattern of high carnegieite, although not a perfect fit, was closer to the observed pattern than was low carnegieite. The presence of nepheline could be definitely ruled out. Since the high form of carnegieite is stable only above 1250°C, it is possible that the gasifier was operated, at least for a short time, above the reported temperature of 1000 ± 150°C. SEM-EDX confirms the existence of a major phase containing Na-Al-Si and a secondary Na-Al phase (Fig. 4).

Since it was reported[1] that the workers complained of chemical irritations when dismantling the failed lining, and since both x-ray and wet chemical analyses detected NaOH, it is reasonable to write the following reaction to describe the corrosion process:

$$11(Al_6Si_2O_{13}) + 26(NaOH) \rightarrow 22(NaAlSiO_4) + 4(NaAl_{11}O_{17}) + 13H_2O$$
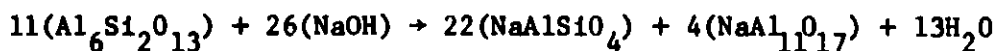
This reaction can be depicted graphically on the $Na_2O-SiO_2-Al_2O_3$ phase diagram (Fig. 5) if Na_2O is substituted for 2NaOH. According to the lever rule, a reaction between a Na compound and mullite should produce $\sim$ 40 wt% β-alumina and 60 wt% carnegieite. If the volume of the Na species is ignored, this reaction has $\sim$ 30% volume expansion associated with it, easily explaining the observed failure.

1

TABLE I. Ash and Slag Compositions of
Indianhead Lignite Coal

Component	Ash	Slag
Na	8.2	6.3
Mg	5.2	6.5
Al	10.6	13.4
Si	21.2	26.0
P	0.9	0.4
S	24.1	9.6
Ca	16.9	23.2
K	0.6	0.2
Ti	0.9	1.0
Fe	10.7	13.0
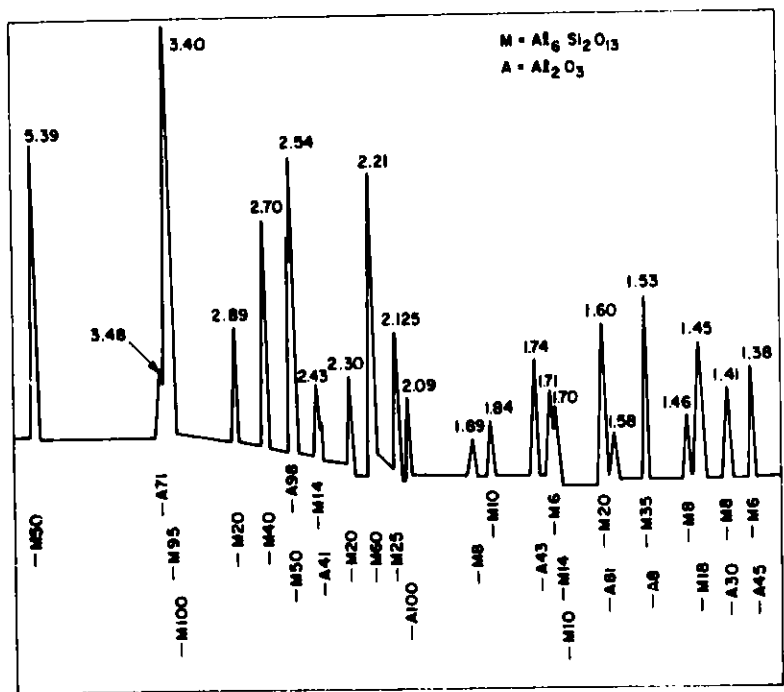
Fig. 1. X-ray Diffraction Pattern Showing Intensity Versus "d" Spacing for
the As-received Mullite Sample. The position and intensity of
the peaks of the mullite (M) and alumina (A) diffraction patterns
are shown at the bottom of the pattern.
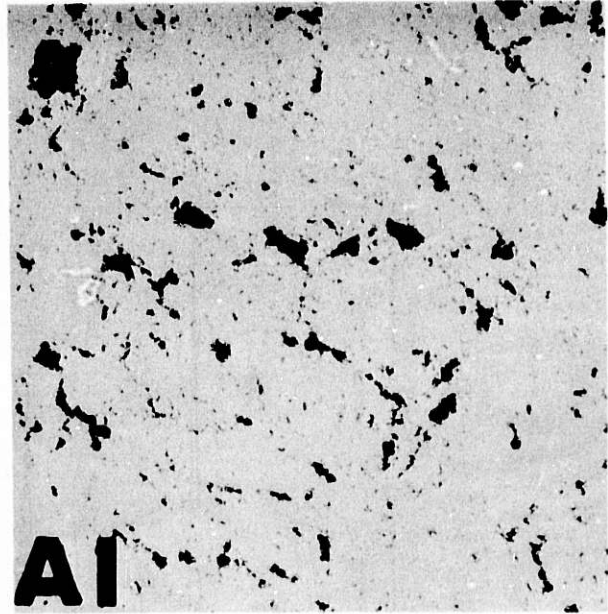
GFETC
MULLITE
AS-RECEIVED
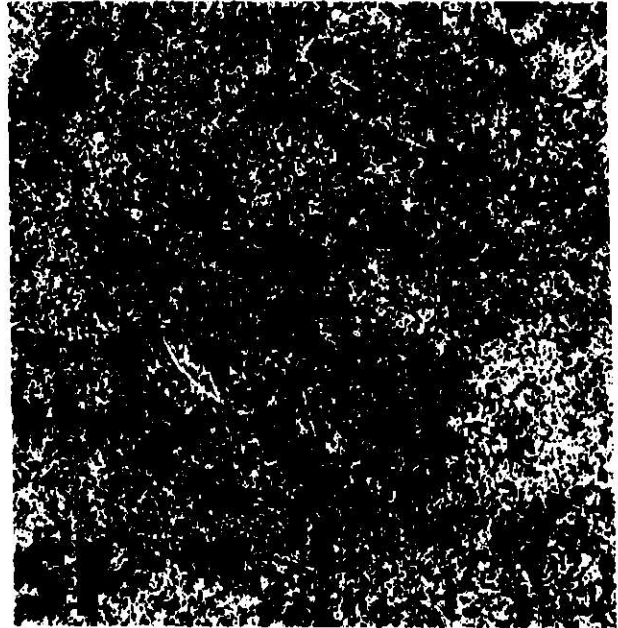
Fig. 2.   SEM Micrograph and Elemental Scans of the As-received Mullite
          Sample. No sodium was detected.
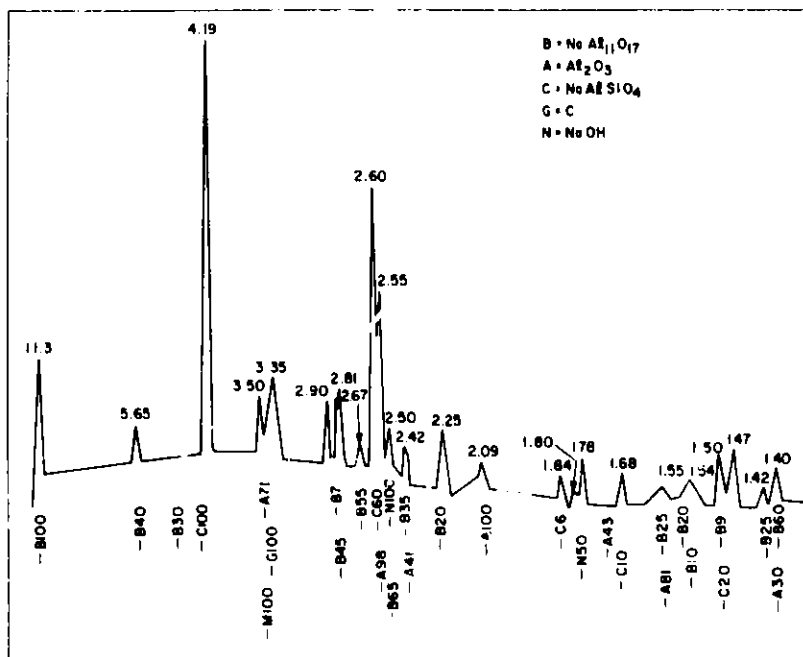
Fig. 3. X-ray Diffraction Pattern Showing Intensity Versus "d" Spacing for the Exposed Mullite Sample. The position and intensity of the peaks or the beta-alumina (B), alumina (a), carnegieite (C), carbon (G), and sodium hydroxide (N) diffraction patterns are shown at the bottom of the pattern.

4
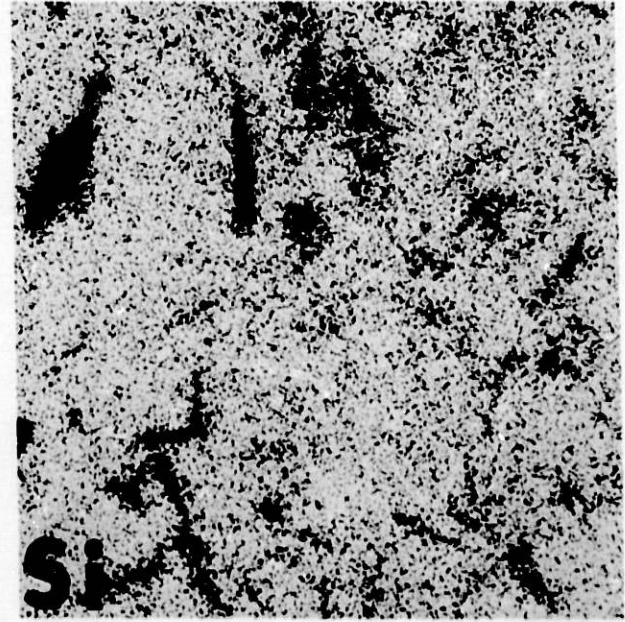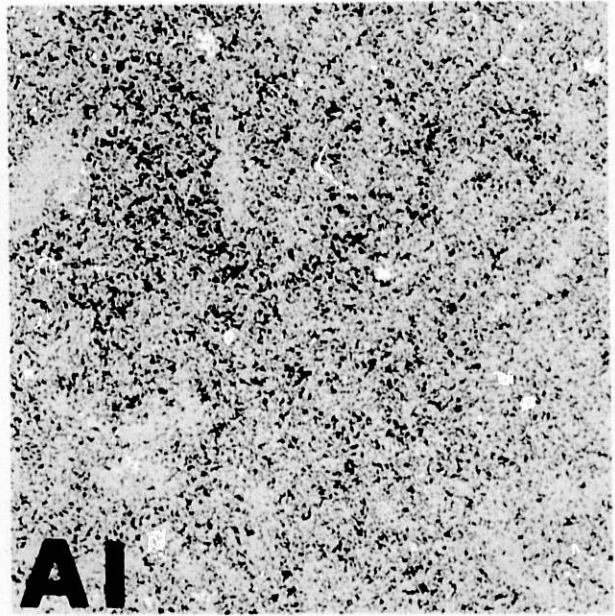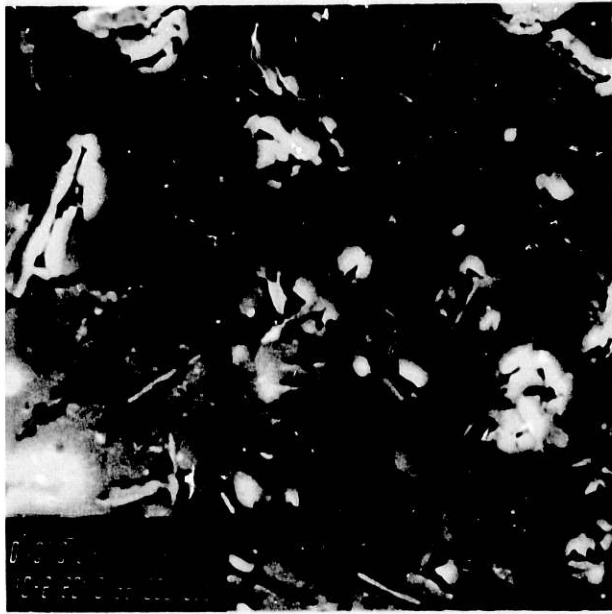
GFETC EXPOSED

Fig. 4. SEM Micrograph and Elemental Scans of the Exposed Refractory Sample.

5
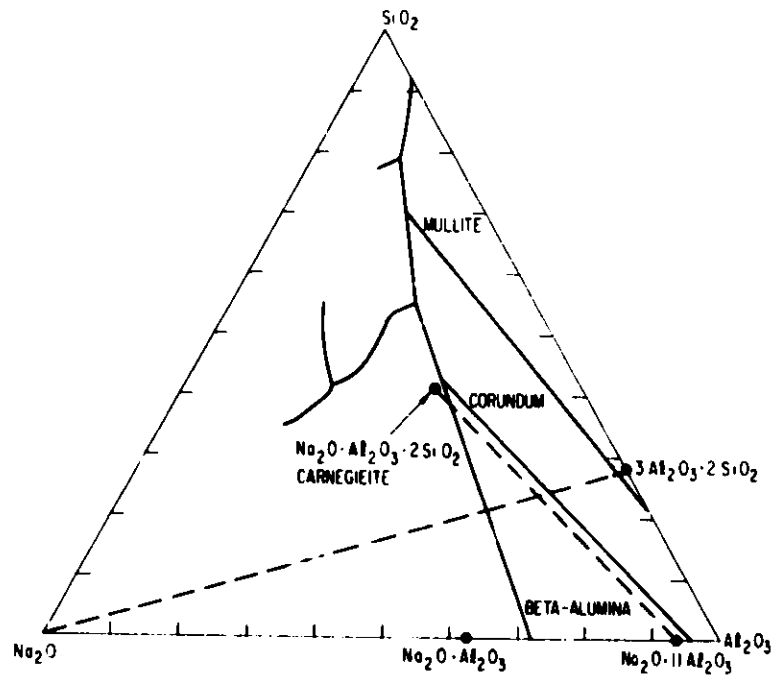
Fig. 5. Equilibrium Phase Diagram of the $Na_2O-SiO_2-Al_2O_3$ System. Dotted lines indicate the reaction according to the "center of gravity" principle.

Task B — <u>Development and Application of Nondestructive Evaluation Methods</u>
<u>for Coal-conversion Processes</u> *(W.A. Ellingson, C.A. Youngdahl,*
D.S. Kupperman, M.J. Caines and N.F. Fiore)

1. **Erosive Wear: Detection and Monitoring**

    a. **Metallic Transfer Lines**

       (1) Ultrasonic Studies - Pilot Plants

       (a) Solvent Refined Coal Liquefaction Plant

       Preparations continued for additional field work at the SRC Pilot
Plant in Ft. Lewis, Wa, as summarized in the previous report[2]. This work is
now scheduled for mid-October and mid-December. Plant personnel are conduct-
ing sequential tests to observe process pipe wear as a function of slurry
velocity and time; thus, at selected sites in the flow system, the previously
instrumented piping will be replaced with smaller-diameter piping in order to
increase the flow velocity for the next stage of the tests. The ANL work
planned for October includes (1) verification of wear indicated by the ANL
automatic erosion scanner during previous plant operations, (2) attachment of
12 new 127-mm (5-in.)-long acoustic waveguides to the 1-1/4-in. (nominal)
Type 321 XXS piping that will replace much of the 2-in. piping of the erosion-
corrosion loop, (3) attachment of three new 5-in. waveguides to new 1-1/2-in.
piping at the preheater outlet, and (4) installation of additional instrument
modules as previously described.[2] Plans for December include instrumentation
of a new preheater coil of 1-1/2-in. piping with four 0.6-m (2-ft.)and two
1.2-m (4-ft.) waveguides.

       The design of the 2- and 4-ft waveguides incorporates (1) a 0.5%
taper in rod diameter over the entire length of the guide in order to prevent
mutual reinforcement of waves interacting with the sidewall and undergoing
mode conversion, which would otherwise interfere with measurements of pipe-
wall thicknesses; (2) a light thread, 0.2 mm (8 mils) deep (32 threads/in.),
on the sidewall to aid in noise reduction; (3) use of ASME 193-B16 alloy
(Fe-1Cr-0.6Mo-0.6Mn-0.4C-0.3V) for most of the length to achieve good high-tem-
perature strength and low acoustic attenuation; and (4) inertial welding (as
previously discussed[3]) or stud welding (to be attempted) to a transition stub
of Type 321 stainless steel at the end of the guide to be attached to piping.
The inertial welding of stubs to the 2-ft. B16 guides has been successfully
accomplished by MTI, Inc., of Mishawaka, IN, at the request of ANL. The large
[15.9-mm (5/8-in.)-dia] end of the bimetallic, tapered waveguides will be
machined for stud welding to piping; the design employs a 7.5-MHz, longi-
tudinal-wave resonant transducer with 9.5-mm (3/8-in.)-diameter crystal at
the smaller end of each guide. The B16 waveguides will be protected from
corrosion by techniques described previously.[3]

       (b) Morgantown Energy Technology Center Fixed-bed Gasifier

       In ANL field work at METC, each of two carbon steel tar-separator
cyclones[2] were equipped with seven 127-mm-long, 9.5-mm-dia (5-in.-long,
3/8-in.-dia) stainless steel acoustic waveguides to permit automatic moni-
toring of wear during a plant operating period which began in August. The
design inlet flow velocity of one of these two cyclones is 91 m/s (300 ft/s);

that of the other, a standby unit, is 61 m/s (200 ft/s). In use, the tar cyclone is located in the gasifier effluent line downstream of the solids-separator cyclone and humidifier stages and is operated at a temperature suitable for the removal of tar as a liquid, i.e., ~ 300°F. The solids- and tar-separator cyclones are both monitored by the ANL ultrasonic wear scanner. The wall thickness of the latter cyclone has been diminishing at a substantial rate during operation, and alternate materials of construction are being considered for a replacement unit. Detailed results of the wear monitoring will be included in a future report.

A cooperative paper, "Erosive Wear and Design Evaluation of a Stainless Steel Cyclone on the Coal Gasification Pilot Facility at Morgantown," by C.A. Youngdahl (ANL), K. Pater (METC), and M.J. Gorski (TRW Energy Systems Group), was presented at the Conference on Properties and Performance of Materials in the Coal Gasification Environment, Pittsburgh, PA, on September 10, 1980.

(c)   Exxon Coal Liquefaction Pilot Plant

Preparations continued for installation of an automatic erosion scanner[2] at ECLP. Waveguides and remote switching modules are to be installed during a plant turnaround period in October or November, and the system is to be made operational after the completion of turnaround activities. Fabrication of six remote switching modules and a switching control module has been completed. Development of pressure-coupling techniques for waveguide monitoring is near completion, and the effects of temperature on acoustic velocity in various metals to be monitored at ECLP have been surveyed.

Development efforts on the high-temperature pressure-coupling techniques included (1) improving the mechanical design of the waveguide clamping fixture, (2) testing couplant materials for use between the waveguide and the outer pipe surface, and (3) minimizing the required contact pressure between the waveguide and pipe wall for reliable ultrasonic signal transmission.

As previously reported[3], the first waveguide-holding fixture utilized a commercially available pipe saddle. When this system was heated to 700°C (~ 1300°F), held at temperature for two hours, and then cooled to room temperature, the pressure at the waveguide contact area was not maintained. To circumvent this problem, a second saddle was designed (Fig. 6); Type 304 stainless steel was selected because of its resistance to creep at the temperatures and stresses for which this system is designed. The maximum stress in the pipe saddles will be ~ 13×10^6 Pa (2000 psi). The new saddle uses Belleville spring washers of Type 302 stainless steel to apply a load to the waveguide. These washers are located on a portion of the saddle which is far enough away from the pipe wall so that they are not exposed to high temperatures which would cause relaxation. To test the performance of the stainless steel pipe saddle, it was heated to 600°C (1100°F), held at temperature for 8 to 16 hours, then cooled to room temperature. This cycle was repeated 11 times over a period of two months without an observable change in pressure, as determined by deflection of the Belleville springs.

Good transmission of ultrasound through the interface between the contact area of the waveguide and the outside surface of the pipe requires that both surfaces be smooth. A roughness of more than approximately 1/10 of

the wavelength of the ultrasound markedly impairs the coupling; the acoustic pressure in the axial direction is reduced and greater lateral scattering occurs.[4] Since the wavelength of the ultrasonic transducers used in this system is ∿ 0.77 mm (∿ 0.030 in.), and the average surface roughness of as-received process piping typically ranges from 10 µm to ∿ 1 mm, the surface must first be polished for good coupling of the ultrasound. Both the contact end of the waveguide and the contact area of the outside pipe wall are polished to the same finish. The polishing process uses several grades of abrasives, graduating to a 1-µm diamond paste. After polishing, the average surface roughness is 0.5- to 0.8-µm.

Because geometrical matching of waveguide to pipe wall is not feasible, a couplant is needed which will not deteriorate over long periods at high temperature with thermal cycling. Various liquids and pastes were evaluated, but none performed for extended periods above 500 °C (∿ 900°F). Several metal foils, including gold, platinum, aluminum, and copper, were also evaluated. It was found experimentally that annealed copper foil with a nominal thickness of 2.5 mm (∿0.010 in.) gave the best ultrasonic coupling with the least amount of coupling pressure, owing to its ductility and low coefficient of reflection. The reflection coefficient for longitudinal waves incident to the boundary between copper and steel is approximately 0.3%.[5] Other benefits of copper foil as a couplant include its low cost and availability. In practice, the copper foil is first annealed to soften it and cleaned to remove surface oxidation. It is then placed between the waveguide and the pipe surface, and compressed with concomitant heating to aid conformation to the outer surface of the pipe. After this procedure, there is relatively little reflection from the interface between the waveguide and the pipe wall (Fig. 7).

An experiment was performed to determine the pressure needed at the contact area of the waveguide, using a copper-foil couplant, in order to transmit enough ultrasound into the pipe wall for reliable erosion/corrosion monitoring. The contact area of the waveguide was a 6-mm (1/4-in.)-dia circle curved to fit the general contour of the pipe wall. Figure 8 graphically shows the results of this experiment; usable signals required pressures of 50 to 70 MPa (7 to 10 ksi).

The effect of temperature on acoustic velocity in piping materials was also investigated. Measurements of longitudinal- and shear-wave velocities were made from 20 to 600°C in Types 304, 316, and 321 stainless steel, C5 cast stainless steel, and 1018 carbon steel. Type C5 wrought stainless steel and CF8M centrifugally cast pipe material remain to be tested. Metallurgical examination of a section of the latter material revealed a columnar grain structure with 1 x 10-mm grains, and zones of smaller grains at the inner and outer pipe surfaces. While this structure may complicate precise ultrasonic measurements, it was possible to examine the material ultrasonically at 7.5 MHz. The velocity vs temperature results for the foregoing materials will be verified and included in a future report.
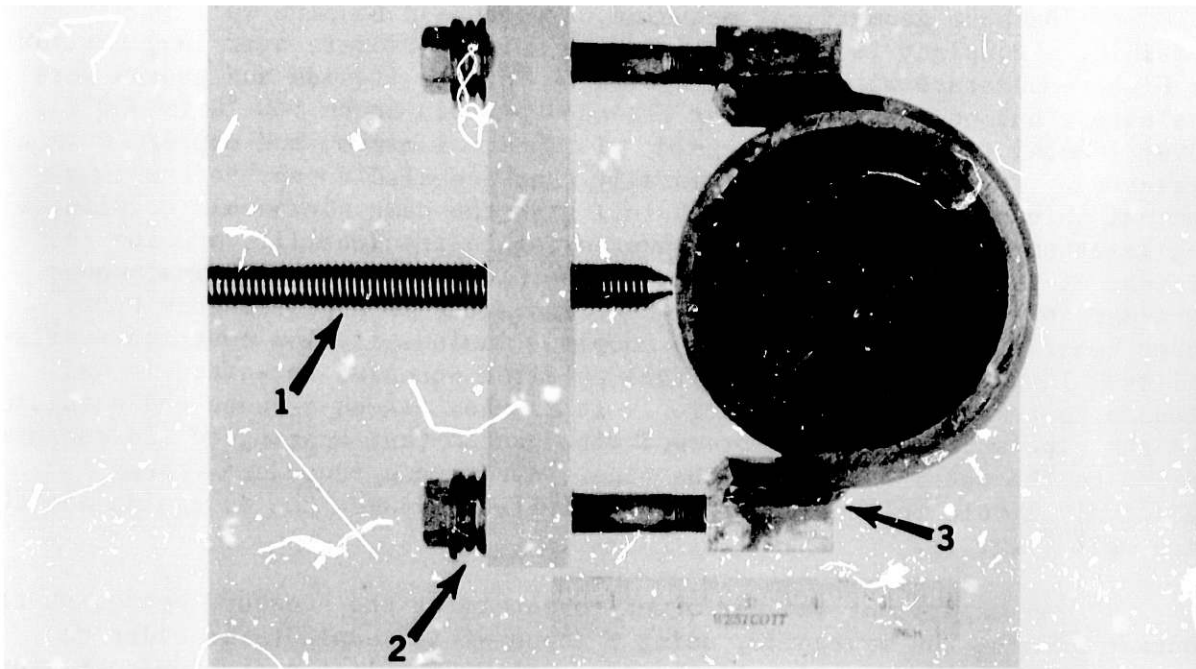
Fig. 6. Pressure-coupled Waveguide Assembly Shown Mounted on Pipe Section.
(1) Type 304 stainless steel waveguide, (2) Belleville spring
washer, (3) pipe saddle.
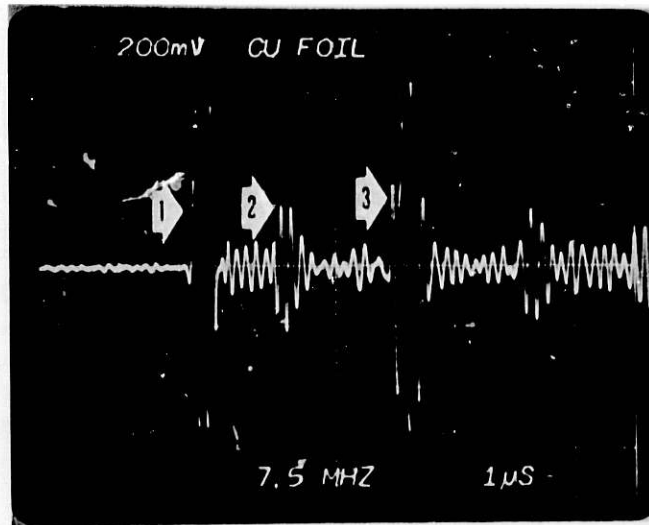
Fig. 7. Photograph of rf Signals from the Waveguide Pressure-coupling System.
(1) Reference signal from the shoulder near the end of the waveguide;
(2) signal from the interface between the waveguide and the outer
pipe surface; (3) signal from the inner pipe surface. Photograph
taken at room temperature with 60 MPa coupling pressure.
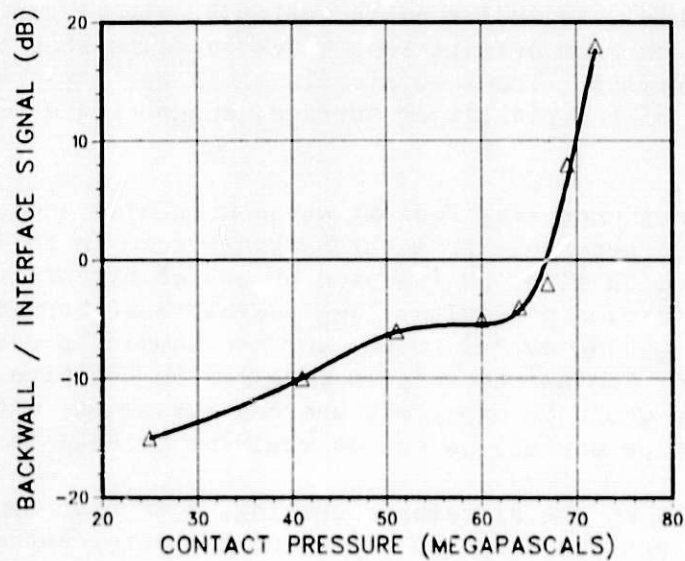
Fig. 8. Ratio of Ultrasonic Signal Reflections from the Inner Pipe Surface
(Backwall) and Waveguide/Outer-pipe-surface Interface, as a
Function of Contact Pressure.

2. Flaw Characterization

a. Ultrasonic NDE Support and Metallographic Studies of Solvent Refined Coal Liquefaction Plant Stainless Steel Pipe

In October 1979, ultrasonic echoes were observed during an in-service ultrasonic shear-wave inspection of a bend in a 4-in. Type 347 stainless steel pipe at the SRC II plant in Ft. Lewis, WA (pipe identification #4-in.-SL-16-A6). The echoes were thought to be from ~ 0.1-mm (0.004-in.)-deep cracks on the pipe inner surface. Argonne National Laboratory was asked to help identify the source of these ultrasonic echoes. A general examination of the elbow section received from SRC indicated a hard scale of varying thickness [generally of the order of 0.13-0.5 mm (5-20 mils)] on the inner surface, but no obvious cracking. An ultrasonic examination of the pipe was carried out at ANL using 45° and 60° angle-beam shear waves operating at frequencies of 2.25 and 10 MHz. Indeed, several echoes were observed, suggesting cracks at the inner surface. However, no cracks were found upon close examination of the specific region where they were expected. This examination included sectioning and grinding of a piece of the piping in an area where a reflector was indicated.

Two flawed areas in another section of the pipe, designated A and B, were also ultrasonically examined. A Sonic Mark III pulser-receiver was employed for the measurements, along with an Aerotech miniature shear-wave transducer. A 0.13-mm (5-mil)-deep saw cut was used as a reference reflector (see Fig. 9). The relative heights of the echo signals obtained with various transducer orientations are recorded in Table II for the saw cut and reflectors A and B. The use of a 60° angle-beam probe reduced the echo signal strength considerably. As indicated in Table II, signal amplitudes were strongly dependent on beam orientation, which suggests that the reflections were not due to porosity. The echo signals could be damped by touching the corresponding area of the pipe inner surface, suggesting a flaw close to the inner surface.

Normal-incidence longitudinal waves were also used, but gave no distinct echo signal separable from the backwall echo in the flawed regions. This lack of resolution might be improved by use of higher-frequency (15 MHz), highly damped (1-2 cycles per pulse) longitudinal-wave transducers. Longitudinal waves propagating normal to the surface should be useful for identifying large voids or laminar-type flaws parallel to the pipe surface. For those flaws, echoes would be expected, whereas for cracks with planes perpendicular to the pipe surface no echoes would be detectable.

Subsequent to the ultrasonic testing, a section containing one of the flawed regions was cut from the pipe, and the outer surface was machined flat to allow better localization of spurious inner-surface reflectors and to eliminate couplant problems associated with a rough, curved surface. A schematic of this specimen is shown in Fig. 10. An artificial electric discharge machined (EDM) notch 0.25 mm deep x 10 mm long x 0.5 mm wide was cut into the inner surface to act as a reference reflector. Figure 11 shows grey-scale recordings of C-scans of the sample, made in two directions. A 10-MHz, 1/2-in. Aerotech immersion transducer was used to generate 45° shear waves. The darkest areas represent a reflector with an echo height equal to 100% of the full screen on the Mark III. The notch is clearly visible in

both scans; a flaw is indicated in only one scan. Part of this flawed area
was interrogated more thoroughly. Figure 12 compares an echo from the ref-
erence notch and an echo from the suspect region. In this case, a 1/4-in.
shear beam at 2.25 MHz was employed. Pulser-receiver settings for notch and
flaw are the same in this comparison. With a 60° angle beam, the flaw signal
could not be seen.

The region containing the flaw indication was examined by metallo-
graphic sectioning. A section of the specimen containing the flaw indication
was mounted in a 25-mm-dia Bakelite block, with the inner surface facing up-
ward. The curvature was ground from the block on 600-grit SiC paper, re-
vealing a 3-mm-long blister in the inner-surface scale (Fig. 13a). The as-
flattened face of the block was defined as zero depth. The blister remained
after further grinding of the surface to depths of ᵥ 0.26 mm (Fig. 13b) and
1.3 mm (Fig. 13c). After the latter grinding step, the blister was examined
at 50X magnification; a tight array of nonmetallic inclusions, each less than
40 μm across, was visible in the metal. These inclusions alone would probably
be too small to cause ultrasonic echo signals with the amplitudes observed in
this study. However, combined with reflections from the blister, the ultra-
sonic signal is detectable. After 4.1 mm was removed from the surface, the
blister was essentially eliminated.

   b. Conclusions

   1. The main conclusion is that ultrasonic shear-wave reflections
       near the inner wall of a pipe cannot be considered a priori
       evidence of cracks. In at least one case, ultrasonic echoes
       detected in a Type 347 stainless steel pipe were reflections
       from a deep subsurface blister containing a cluster of
       nonmetallic particles. The cluster may have been present in
       the steel as a result of processing (e.g., trapped slag). Once
       in the steel, it may have served as a preferred scale-buildup
       site and caused the large blister to form; alternatively, the
       cluster may have formed as a result of scale buildup, and may
       represent accelerated localized oxidation.

   2. The use of both 45° and 60° angle-beam probes during shear-wave
       ultrasonic testing is recommended to help increase the proba-
       bility of identifying the cause of reflections. Crack-like
       flaws at the inner surface will probably cause detectable
       ultrasonic echoes with both 45 and 60° probes (as do EDM
       notches); however, other types of flaws, such as those found in
       the present examination, may not be detected or may generate
       much weaker signals with the 60° probe than with the 45° probe.

   3. Normal-incidence longitudinal waves (up to 15 MHz) should also
       be used to interrogate a suspect pipe region. With normal-
       incidence longitudinal waves, the presence of echoes not
       identified as inner-wall reflections would indicate laminar-
       type defects, voids, or blisters. However, depending on the
       equipment used, such defects could also be present without
       generating discernible longitudinal-wave echoes, as in the
       example reported here.

TABLE II. Relative Echo Heights Obtained from Three Different Reflectors
During Ultrasonic Examination[a] of the Type 347 Stainless Steel
Pipe Section Shown in Fig. 9

Reflector	Beam Angle, Degrees	Beam Direction, Degrees	Relative Signal Amplitude
0.13-mm-deep saw cut	45	270	30
	60	270	20
A	45	300	40
	60	300	20
B	45	300	25
	60	–	0

[a]Pulse-echo mode (2.25-MHz, 1/2-in. single-element transducer).
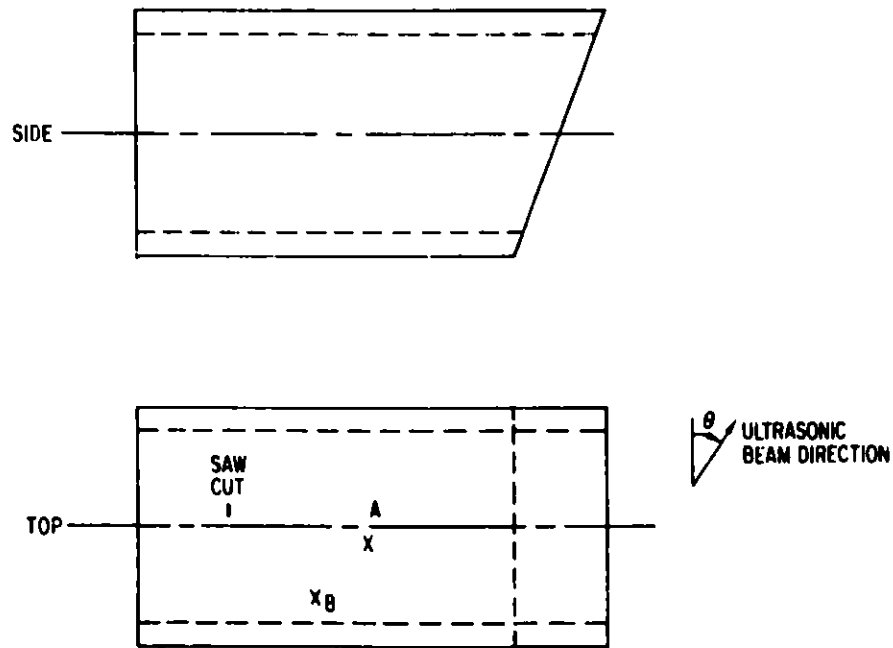
Fig. 9. Schematic of Type 347 Stainless Steel Pipe Section, Showing Lo-
cations of 0.13-mm (5-mil)-deep Saw Cut and Two Flaw Indications
(A and B).

EDM NOTCH ON I.D.
(0.025 DEEP, I L__ __ 0.05 WIDE)

11.25
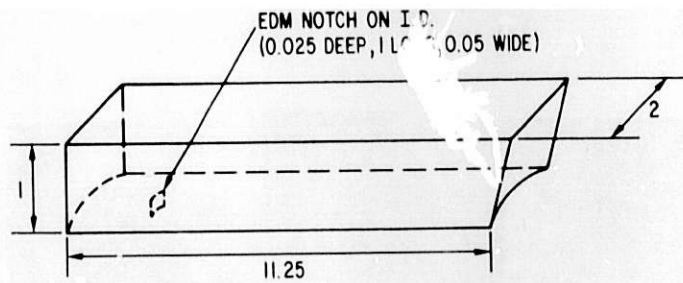
Fig. 10. Schematic of Specimen Cut from Pipe Sample of Fig. 9. The inner surface has been left intact, while the outer surface has been machined flat. Dimensions in cm.

◄— SCAN DIRECTION

EDM NOTCH   FLAW   END

45° Shear Wave
10-MHz Transducer

EDM
NOTCH   END
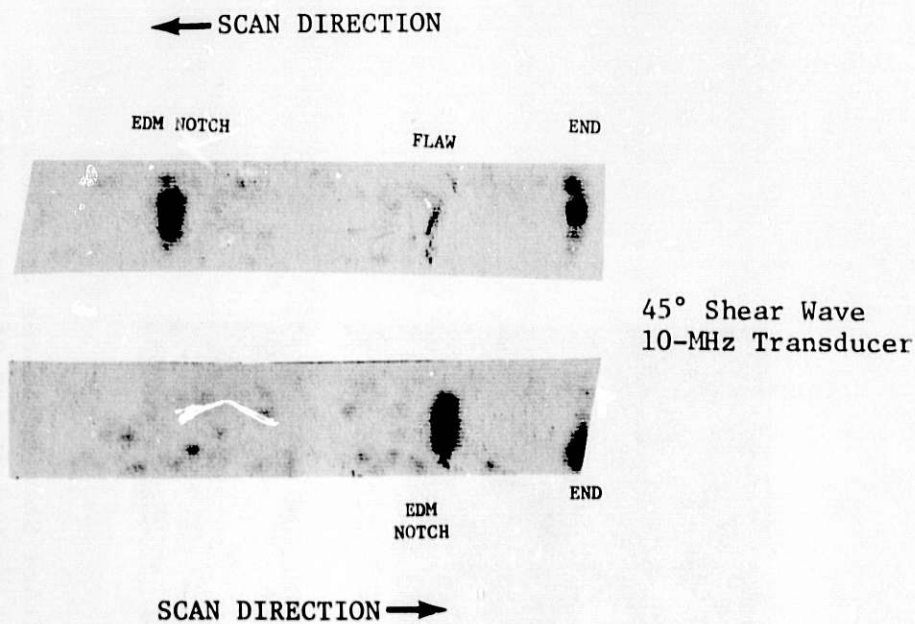
SCAN DIRECTION —►

Fig. 11. Gray-scale C-scan Recordings of Specimen Shown in Fig. 10. Two scan directions are indicated. A 10-MHz, 1/2-in.-dia Aerotech immersion transducer was used to generate 45° shear waves.

15

EDM
NOTCH
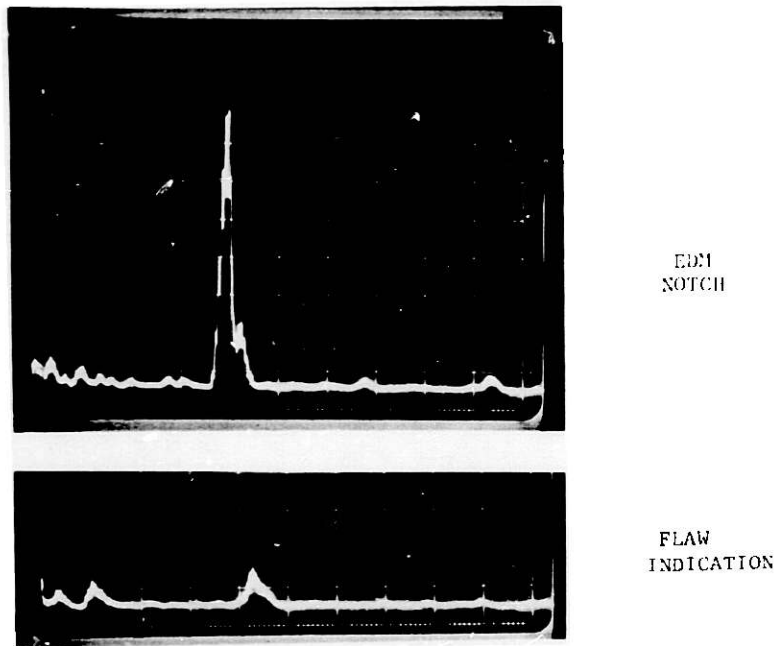
FLAW
INDICATION

Fig. 12. A-scan Trace Showing Echoes from Reference
Notch and Flawed Region of Pipe Section
Shown in Fig. 10. A 2.25-MHz, 1/4-in.-dia
Aerotech miniature 45° shear-wave transducer
was employed. Beam direction (along the
pipe axis) and equipment settings are the
same for both traces.

0 depth

0.26 mm deep

1.3 mm deep
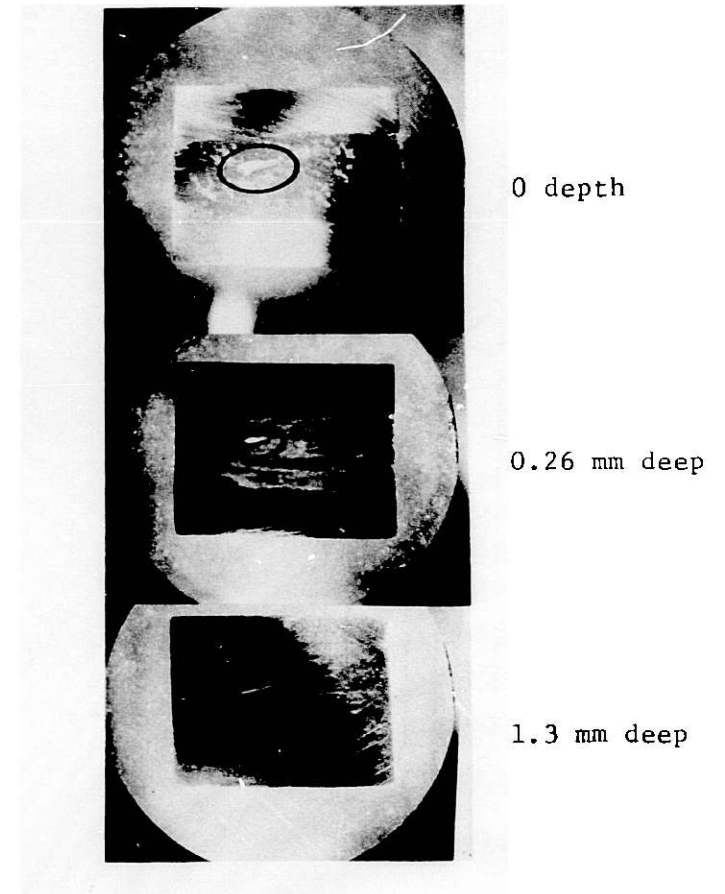
Fig. 13. Cross Section of Blister at
Various Depths of Grinding. The
circular field of view is 25 mm
in diameter.

3. Refractory Installation Practices

a. Detection of Thermally Induced Acoustic Emissions from Refractory Concrete Materials

Recent work in Japan[6] on the use of acoustic-emission detection to assess the spalling potential of refractory linings for blast furnaces has given excellent results. Kumagai et al.[6] reported that acoustic-emission methods were capable of identifying suitable bricks for blast-furnace linings. These tests involved magnesia-dolomite bricks as well as bricks with magnesia-carbon content. As discussed in earlier reports in this series,[2,7] acoustic-emission detection is expected to be a valuable tool for the control of firing schedules for refractory linings, as well as the determination of spalling potential. This is especially critical for closed vessels that will not be reopened prior to use.

4. Component Inspection

a. Acoustic Valve Leak Detection

The previous report[2] described the selection of five valves for monitoring at the Exxon Donor Solvent Plant in Baytown, TX, and results of theoretical work which addressed the problem of quantifying leakage rates by nonintrusive acoustic emission techniques. This work suggested that low-mass-flow measurement methods would have to be coupled with noninvasive acoustic systems to quantitatively measure liquid leakage.

During the present quarter, a preliminary design was completed for a slurry test loop. This will allow tests to be conducted for the detection of liquid slurry leaks under conditions of $\Delta P \sim 3.4$ MPa (500 psig), a temperature of 427°C (800°F), run times of 15-60 s, and a range of flow rates. Figure 14 shows a schematic of the proposed flow loop and instrumentation. Final design and construction should be initiated in the next quarter.

GUIDE
ELECTRONIC COUNTER
(GIVES PISTON DISPLACEMENT/VELOCITY)
VARIABLE-SPEED GEAR BOX
10-HP ELECTRIC MOTOR
THREADED ROD
VALVE
NICHROME WIRE HEATING ELEMENT
76 mm
HYDRAULIC RAM 152 mm DIAMETER
HIGH-TEMPERANCE KAPOK INSULATION
THERMOCOUPLE
PRESSURE GAUGE
76 mm
TEST SECTION 76 mm
1/4-HP SEALED ELECTRIC MOTOR
COOLANT FOR MOTOR
CROSS-CORRELATION FLOWMETER
SURFACE-MOUNTED THERMOCOUPLES (3)
PRESSURE GAUGES
IMPEDANCE-TYPE (PHASE SHIFT) FLOWMETER
OSCILLATOR
PRESSURE REGULATOR
QUICK-OPENING (POP) VALVE
3 1/2-HP STD SHOP COMPRESSOR (0.7 MPa; 100 psig)
1-HP STD COMMERCIAL MIXER
5-kJ HEATING ELEMENT
STORAGE TANK 0.3 m DIAMETER 3.0 m HIGH
152 mm INSULATION
51 mm DIAMETER
VALVE
0.5-HP PUMP
DIAMETRICALLY OPPOSED PRESSURE TRANSDUCERS
RADIAL OUTFLOW
VENT
ANECHOIC TERMINATION (REMOVABLE)
1/4-HP PUMP

OPERATING CONDITIONS:
MAX. TEMPERATURE : 400°C (800°F)
MAX. PRESSURE : 3.5 MPa (500 psi)
RUN TIME : 15-3700 s
OIL DENSITY : 480-900 kg/m³ (30 < ρ < 56 lbf/ft³)
OIL VISCOSITY : 3-240 cp (7×10⁻⁵ < μ < 5×10⁻³ lbf·s/ft²)
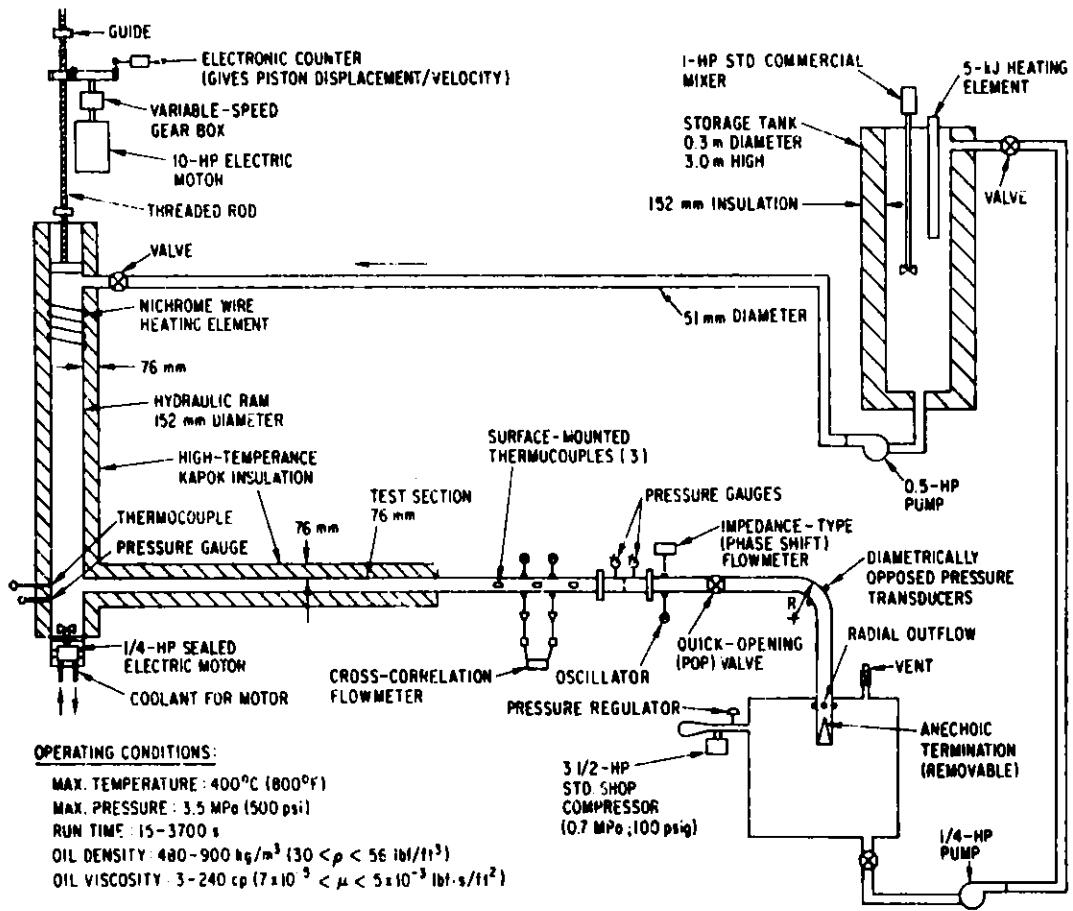
Fig. 14. Schematic of Test Apparatus for Detection of Liquid Slurry Leaks.

18

Task C -- <u>Corrosion Behavior of Materials in Coal-conversion Processes</u>
        (K. Natesan)

The objectives of this program are to (1) develop uniaxial tensile data on four selected commercial alloys exposed to multicomponent gas environments, (2) experimentally evaluate the high-temperature corrosion behavior of iron- and nickel-base alloys in gas environments with a wide range of oxygen, sulfur, and carbon potentials, (3) evaluate deposit-induced hot-corrosion behavior of heat-exchanger and gas-turbine materials with and without coatings after exposure to multicomponent gas environments, and (4) develop an approach that is based upon available thermodynamic and kinetic information for evaluating possible corrosion problems in various coal-conversion systems.

Deposit-induced corrosion behavior of heat-exchanger and gas-turbine materials exposed to multicomponent gas environments is of considerable interest in advanced energy systems that utilize fossil fuels. For this reason, the ongoing program includes characterization of environments in low-Btu gasification and direct-combustion processes and the evaluation of materials in complex gas mixtures that simulate normal operating conditions and off-normal excursion situations in these processes.

To simulate the air and steam tubes exposed in an environment from combustion of coal or coal-derived fuels, tube specimens that are internally cooled with air or inert gas are used in a series of corrosion experiments. Details of the experimental apparatus to evaluate the corrosion behavior of selected materials over the temperature regimes of interest in combustion systems were given in an earlier quarterly report.[8] The chemical compositions of the alloys used in these experiments are given in Table III. The experimental conditions and the calculated values of oxygen, sulfur, sulfur dioxide, and sulfur trioxide partial pressure are shown in Table IV. The calculations were made using the equilibrium computer code developed at ANL. Experiments have been conducted with metal temperatures of 866 and 977 K (593 and 704°C) and gas temperatures between 971 and 1123 K. In some runs, Incoloy 800 specimens that had been coated with $CaSO_4$ (simulating sulfated limestone deposits) were exposed to the complex gas mixtures to evaluate the influence of sorbent material on the corrosion behavior of the materials. The exposure times in various runs were in the range 400 to 500 h.

The gas environments in the present experiments were such that the partial pressures of oxygen corresponded to combustion stoichiometric ratios (SRs) greater than 1.0. Figure 15 shows the effects of temperature and combustion SRs on the oxygen and sulfur partial pressures in the gas environment for Montana Rosebud coal. SR values < 1.0 and > 1.0 correspond to air-deficient and excess-air combustion conditions, respectively. The oxygen and sulfur partial pressures established in various experimental runs are shown by closed circles with run numbers. Similar information for partial pressures of sulfur dioxide and sulfur trioxide is shown in Fig. 16. The figures show that the partial pressure of SO_2 in the gas phase will be in the range of 10^{-3} to 10^{-2} atm (10^2 to 10^3 Pa; 1000 to 10,000 ppm) for combustion SR values between 1.02 and 1.30. The partial pressure of SO_3 in the gas phase under these conditions will be 10^{-4} atm (10 Pa; 100 ppm) or less at temperatures of 700°C or higher; however, as the temperature decreases below 700°C, the SO_3 pressure increases to values in the range 10^{-3} to 10^{-2} atm

$(10^2$ to 10^3 Pa; 1000 to 10,000 ppm). In general, the corrosion behavior of a material is strongly influenced by both the metal temperature and SO_3 partial pressure. The effect of these variables on corrosion will be examined in the present program.

Figure 17 shows the various alloy specimens after exposure at 977 K to mixed-gas environments with a wide range of oxygen and sulfur partial pressures. The carbon steel and Fe-2-1/4Cr-1Mo steel specimens in all the runs (except run 114) underwent a sulfidation mode of attack with significant swelling of the alloys. The other, higher-chromium alloys exhibited the oxidation mode of interaction in these environments. In run 114, all the alloys exhibited oxidation; friable iron oxide was produced with low-chromium alloys, and adherent chromium-rich oxide with high-chromium alloys.

Upon completion of the exposures, cross sections of the tube specimens were examined by SEM-EDX to identify the type and location of different elements and phases in the scale layers. Figures 18 to 21 show the specimen images and the elemental mapping for Fe-2-1/4Cr-1Mo steel, Fe-9Cr-1Mo steel, Type 310 stainless steel, and Incoloy 800 after exposure to a gas mixture in run 106. The gas-side interaction in Fe-2-1/4Cr-1Mo steel produced predominantly iron oxide with an inner layer of (Fe,Cr) sulfide, indicating that the iron oxide scale is not impervious to sulfur transport. An (Fe,Cr) oxide phase is observed ahead of the sulfide layer. The results, in general, suggest negligible chromium mobility even at 977 K, primarily owing to the low level in the original alloy. The air-side oxidation of the material results in an ∿ 300-μm-thick layer of iron oxide with virtually no chromium in the scale. The gas-side interaction of Fe-9Cr-1Mo steel resulted in essentially the same morphological features (Fig. 19) as in Fe-2-1/4Cr-1Mo steel. In the case of Type 310 stainless steel (Fig. 20), significant transport of nickel to the intermediate sulfide layer is observed, even though the outer layer was predominantly iron oxide and the layer at the scale/alloy interface was chromium-rich oxide with some sulfur permeation. In contrast to Type 310 stainless steel, the Alloy 800 specimen (Fig. 21) exhibits predominantly (Cr,Fe) oxide with significant sulfur in the scale. A comparison of Figs. 20 and 21 shows that the innermost layer in Type 310 stainless steel and the outer layer in Incoloy 800 are identical. Additional experimental data (as a function of temperature, gas chemistry, and thermal gradient) are required to establish whether the observed enhanced transport of nickel in Type 310 stainless steel is a phenomenon that occurs only in iron-base alloys in the presence of a thermal gradient; however, the experimental results clearly show that iron oxide, if formed as an external scale, is not impervious to transport of sulfur.

Figures 22 and 23 show the morphological features of scales developed on carbon steel, Type 310 stainless steel, and Fe-9Cr-1Mo steel after an ∿ 500-h exposure to gas mixture in run 109. The combination of higher oxygen pressure and lower sulfur pressure in the gas phase results in a chromium-rich oxide layer in both the chromium-containing steels. The behavior of carbon steel was essentially the same as that observed for Fe-2-1/4Cr-1Mo steel in run 106. Even with significantly lower sulfur pressure (run 104), both the __on steel and Fe-2-1/4Cr-1Mo steel (Figs. 24 and 25, respectively) exhibited significant sulfidation, while alloys such as Fe-9Cr-1Mo, Type 310 stainless steel, and Incoloy 800 (Figs. 26 and 27) exhibited oxidation similar to that observed in run 109. The specimens from

runs 110 and 114 and the CaSO$_4$-coated specimens from runs 111 and 112 are presently being analyzed, and the results will be presented in a future report.

TABLE III. Chemical Composition of Alloys Used in Corrosion Experiments

Material	Composition (Mass %)						
	C	Cr	Ni	Mn	Si	Fe	Other
Carbon Steel	0.18	--	--	0.3	0.2	Balance	--
2-1/4Cr-1Mo	0.11	2.3	--	0.8	0.3		--
9Cr-1Mo	0.10	9.0	--	--			--
Type 310 SS	0.15	25.0	20.0	1.5	0.4		--
Incoloy 800	0.05	21.0	32.5	0.75	0.35		0.4 Ti, 0.4 Al

TABLE IV. Experimental Conditions[a] Used in Various Corrosion Runs

Run No.	Partial Pressure (atm)[b]				Temperature (K)	
	O_2	S_2	SO_2	SO_3	Gas	Metal
101	1.3×10^{-10}	1.3×10^{-11}	3.3×10^{-1}	5.9×10^{-6}	1013	866
102	3.1×10^{-10}	7.4×10^{-17}	3.5×10^{-3}	1.1×10^{-7}	1000	866
108[c]	1.9×10^{-10}	1.3×10^{-16}	3.5×10^{-3}	9.5×10^{-8}	993	866
111[c]	1.3×10^{-10}	1.3×10^{-11}	3.3×10^{-1}	5.9×10^{-6}	1013	866
113	1.4×10^{-1}	5×10^{-35}	1.8×10^{-3}	1.7×10^{-3}	971	870
104	2.7×10^{-8}	1.0×10^{-17}	3.5×10^{-3}	4.2×10^{-7}	1085	977
106	6.1×10^{-10}	1.0×10^{-11}	3.3×10^{-1}	8.7×10^{-6}	1048	977
107[c]	1.1×10^{-9}	9.9×10^{-12}	3.3×10^{-1}	1.0×10^{-5}	1063	977
109	1.1×10^{-8}	8.7×10^{-12}	3.3×10^{-1}	1.7×10^{-5}	1123	977
110	1.4×10^{-7}	2.8×10^{-18}	3.5×10^{-3}	7.3×10^{-7}	1113	977
112[c]	1.4×10^{-7}	2.8×10^{-18}	3.5×10^{-3}	7.3×10^{-7}	1113	977
114	1.4×10^{-1}	2.9×10^{-31}	2.8×10^{-3}	7.4×10^{-4}	1088	977

[a]The exposure times in these runs ranged between 400 and 500 h.

[b]Conversion factor: 1 atm = 1.013 x 10^5 Pa.

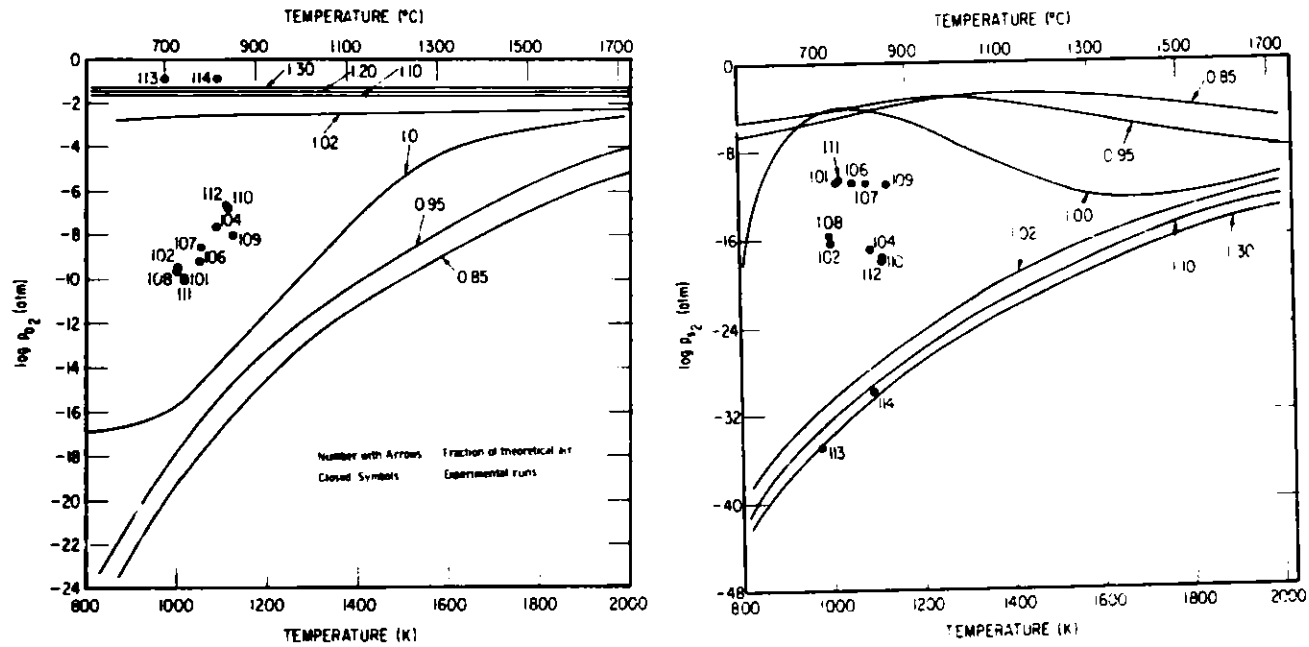[c]Tests conducted with Incoloy 800 specimens coated with $CaSO_4$.

Fig. 15. The Effects of Temperature and Combustion Stoichiometric Ratio (SR) on the Oxygen and Sulfur Partial Pressures in the Gas Environment for Montana Rosebud Coal. SR values < 1.0 and > 1.0 correspond to air-deficient and excess-air combustion conditions, respectively. The conditions in various experimental runs are indicated by closed circles with run numbers. Conversion factor: 1 atm = 1.013×10^5 Pa.
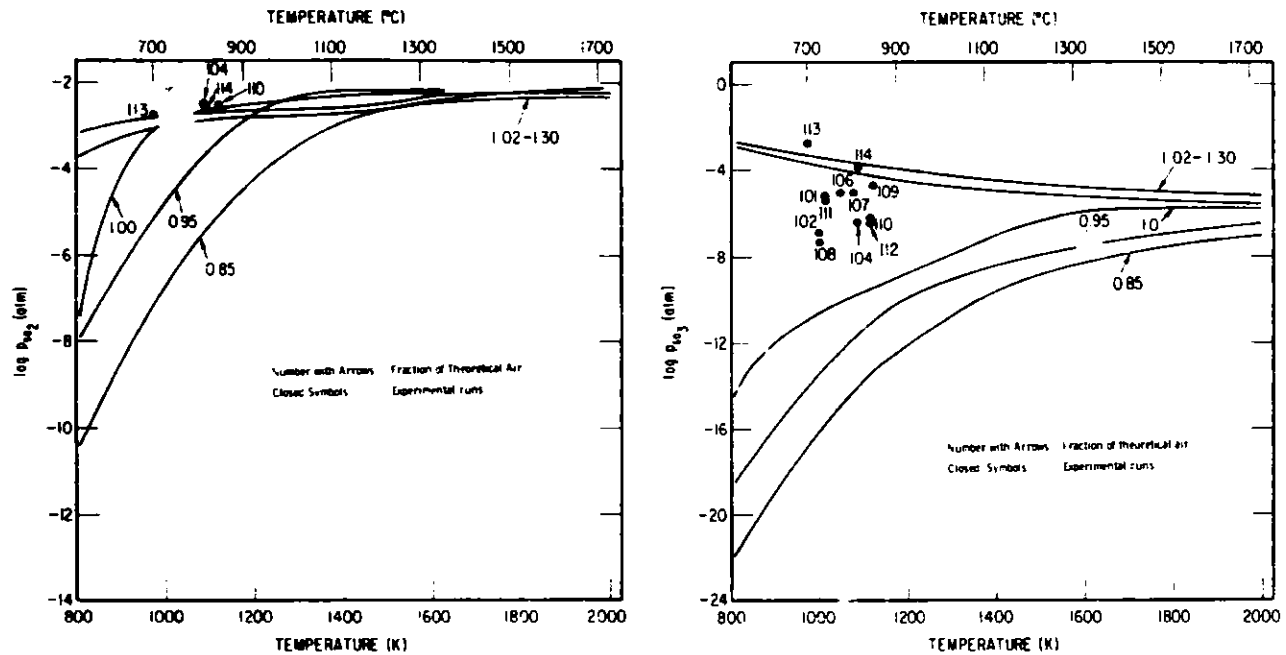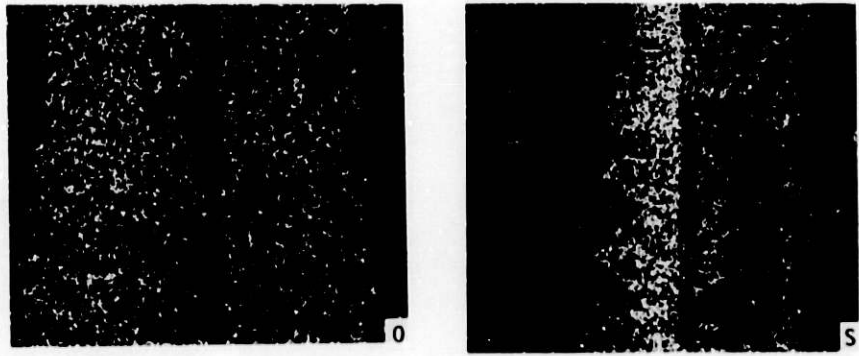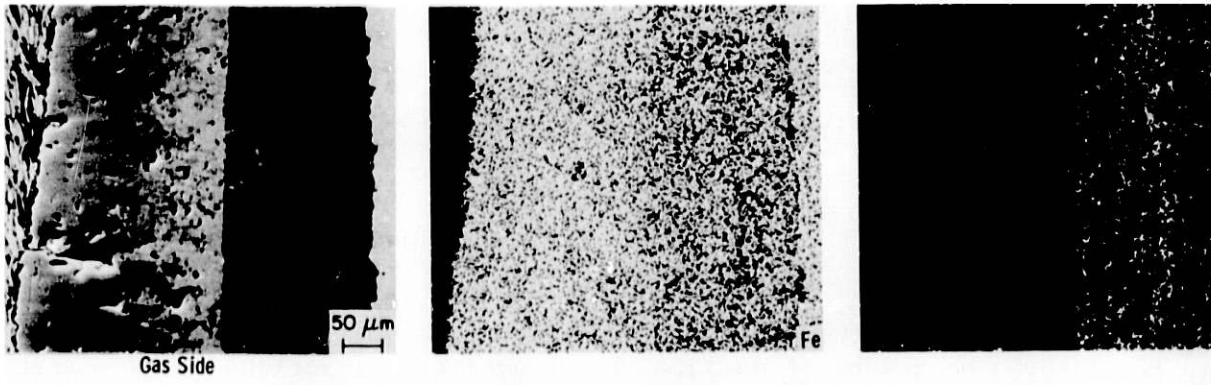
Fig. 16. The Effects of Temperature and Combustion Stoichiometric Ratio (SR) on the SO_2 and SO_3 Partial Pressures in the Gas Environment for Montana Rosebud Coal. SR values < 1.0 and > 1.0 correspond to air-deficient and excess-air combustion conditions, respectively. The conditions in various experimental runs are indicated by closed circles with run numbers. Conversion factor: 1 atm = 1.013 x 10^5 Pa.

Fig. 17. Macrophotographs of Uncoated Tube Specimens of Various Alloys after 500-h Exposure to Mixed-gas Environments with Various Oxygen and Sulfur Partial Pressures.

Fig. 18. SEM Micrograph and Elemental Scans of Fe-2$\frac{1}{4}$Cr-1Mo Steel after a 500-h Exposure in Run 106. Conversion factor: 1 atm = 1.013 x 10^5 Pa.

Fig. 19. SEM Micrograph and Elemental Scans of Fe-9Cr-1Mo Steel after a 500-h Exposure in Run 106. Conversion factor: 1 atm = 1.013 x 10^5 Pa.

Gas Side

Air Side

Run 106   Type 310 ss   Gas Temperature 1048 K $p_{O_2} = 6.1 \times 10^{-10}$ atm
                          Metal Temperature 977 K $p_{S_2} = 1.0 \times 10^{-11}$ atm

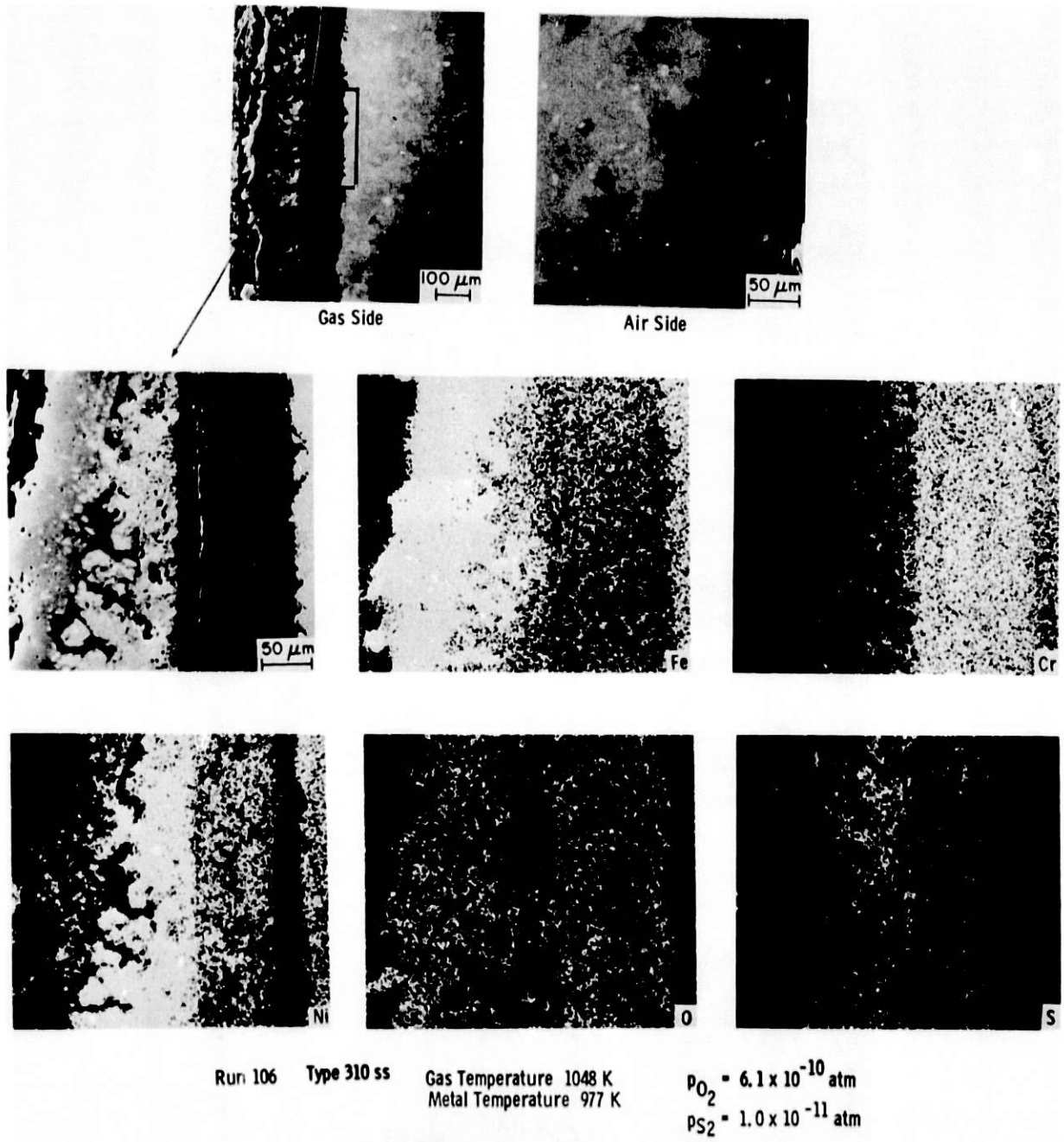Fig. 20.   SEM Micrographs and Elemental Scans of Type 310 Stainless Steel
            after a 500-h Exposure in Run 106.   Conversion factor: 1 atm =
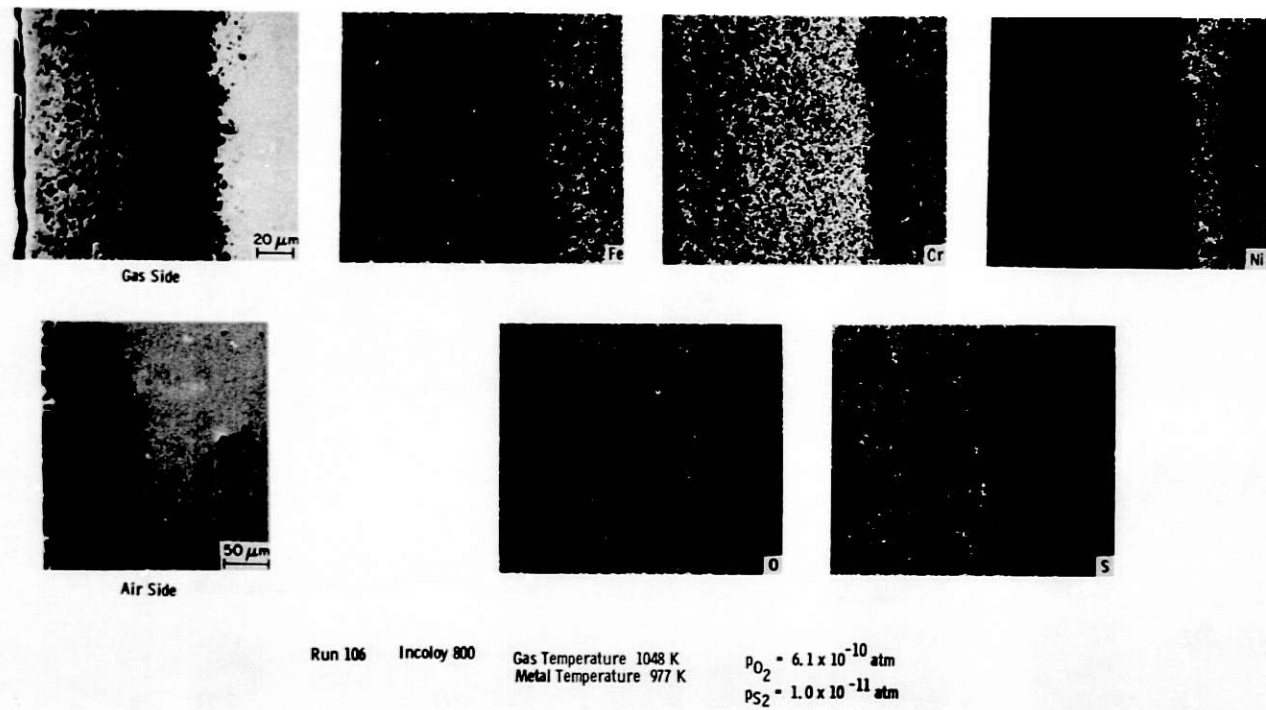 1.013×10^5 Pa.

27

Gas Side

Fe

Cr

Ni

Air Side

O

S

Run 106   Incoloy 800   Gas Temperature 1048 K $p_{O_2} = 6.1 \times 10^{-10}$ atm
                           Metal Temperature 977 K $p_{S_2} = 1.0 \times 10^{-11}$ atm

Fig. 21.   SEM Micrographs and Elemental Scans of Incoloy 800 after a 500-h Exposure in Run 106. Conversion factor: 1 atm = 1.013 × 10^5 Pa.

28

Run 109   Carbon Steel

Gas Temperature 1123 K

Metal Temperature 977 K

$p_{O_2} = 1.1 \times 10^{-8}$ atm

$p_{S_2} = 8.7 \times 10^{-12}$ atm

Gas Side

Air Side
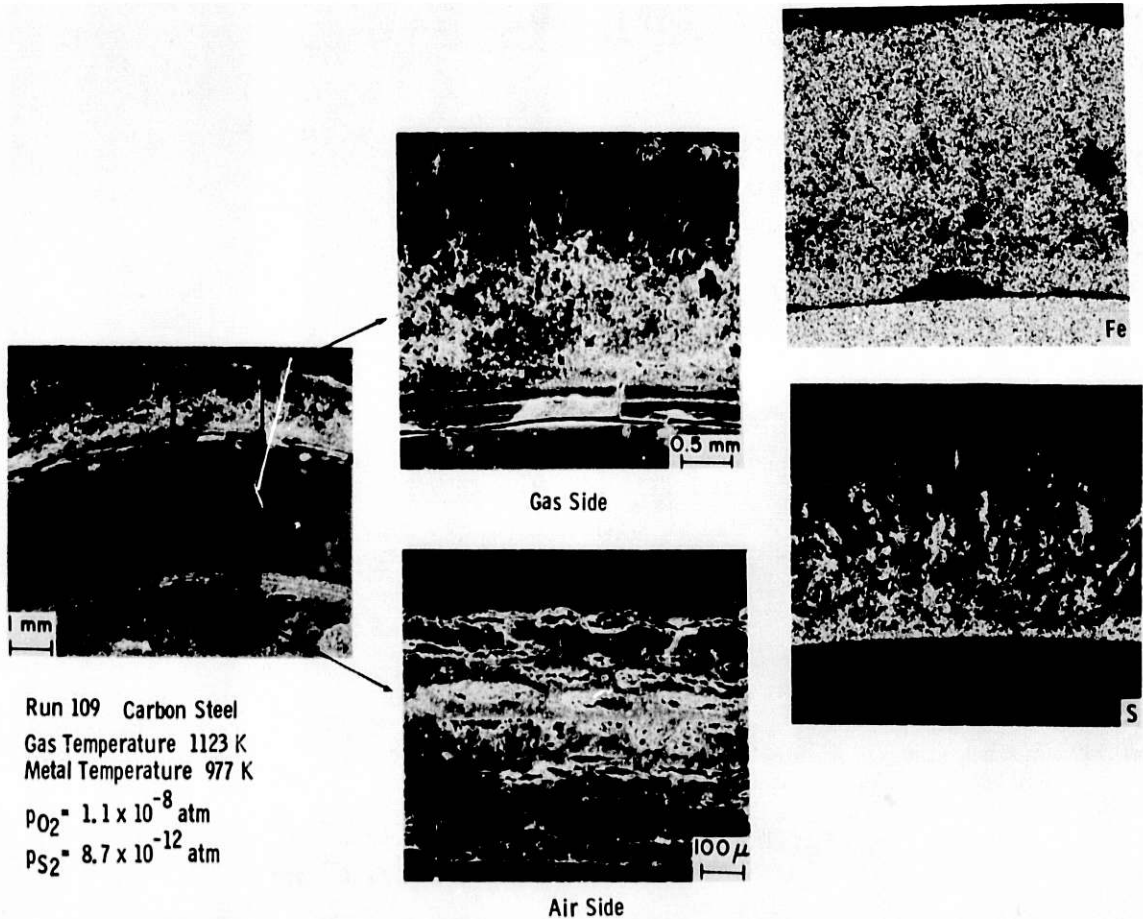
Fig. 22.   SEM Micrographs and Elemental Scans of Carbon Steel after a 500-h Exposure in Run 109.   Conversion factor: 1 atm = 1.013×10^5 Pa.

Gas Side   Cr   Type 310 ss   Fe   Air Side

Gas Side   Cr   Fe- 9 Cr- 1 Mo   Fe   Air Side

Run 109   Gas Temperature 1123 K p_{O2} = 1.1×10^{-8} atm
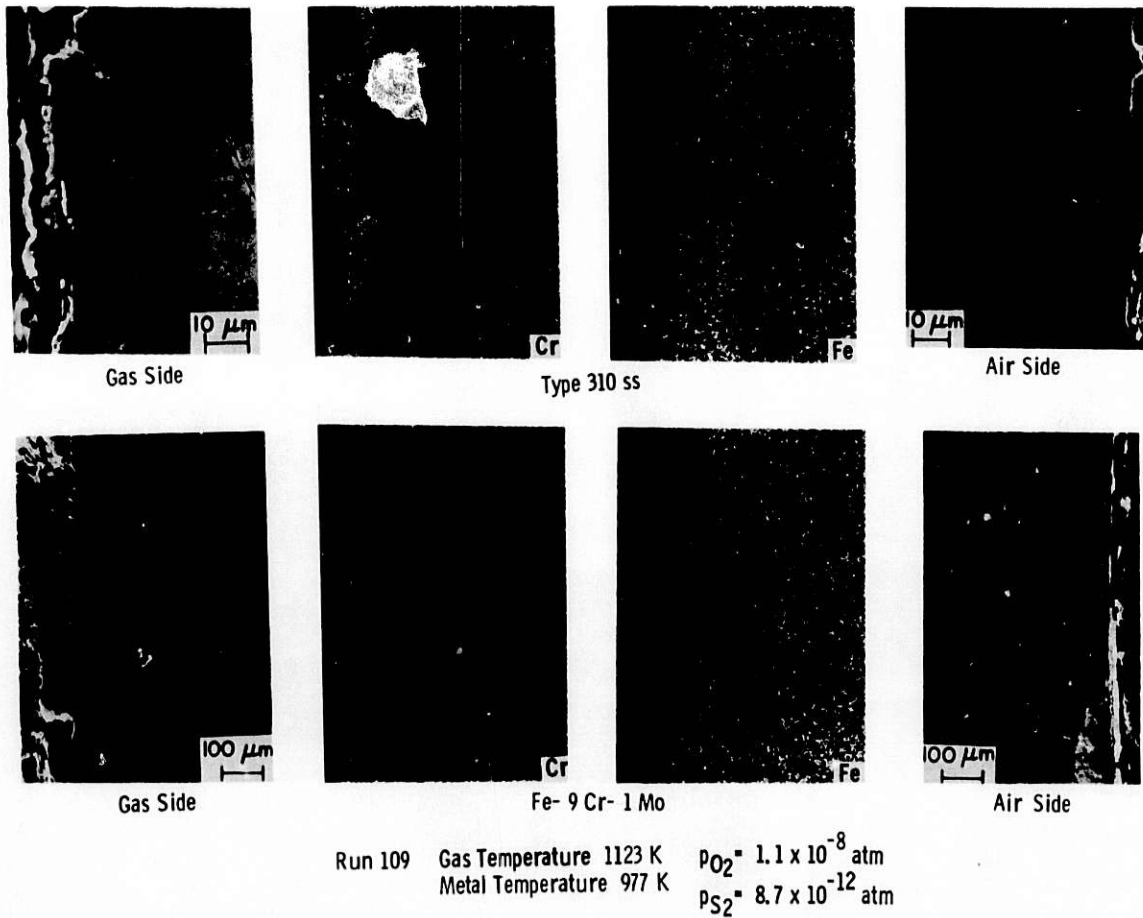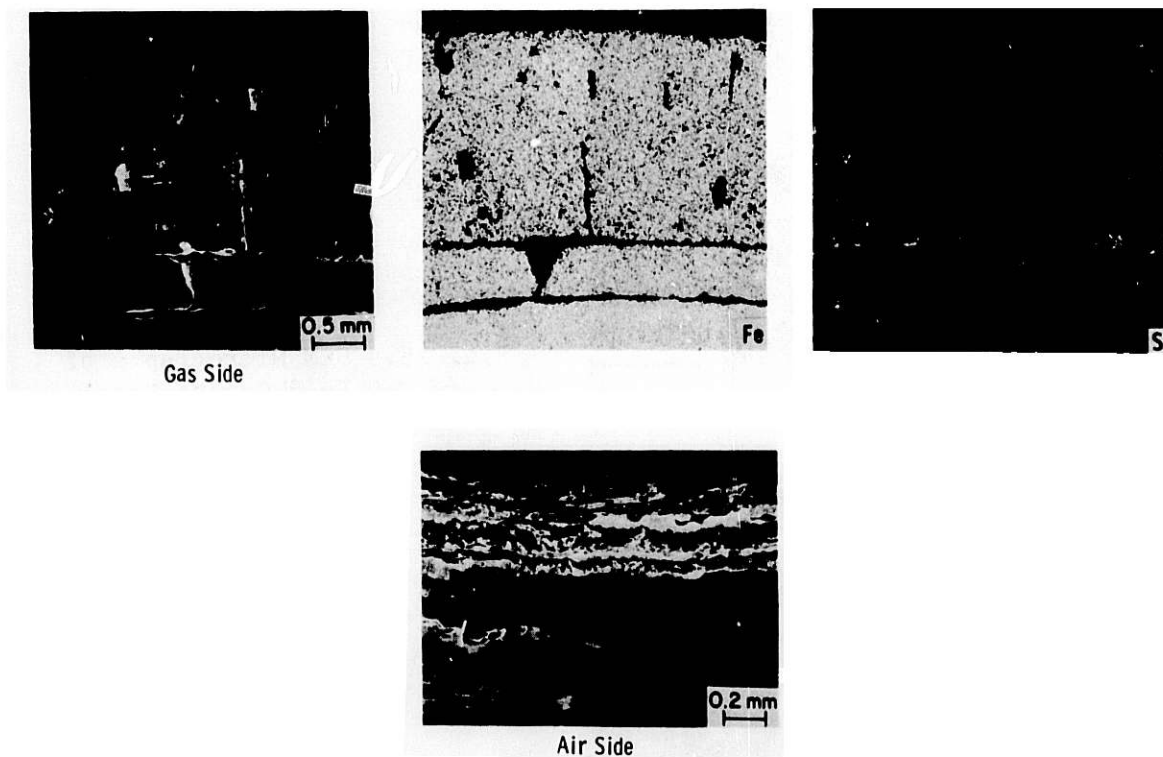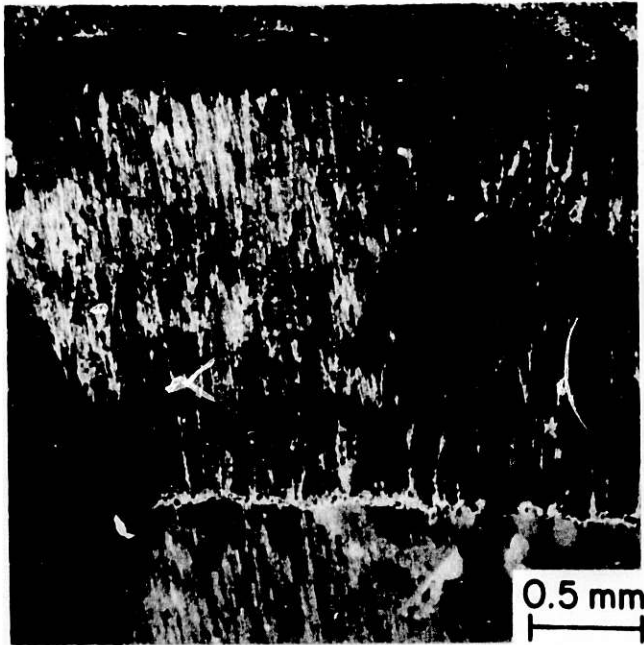Metal Temperature 977 K p_{S2} = 8.7×10^{-12} atm

Fig. 23.   SEM Micrographs and Elemental Scans of Type 310 Stainless Steel and Fe-9Cr-1Mo Steel after a 500-h Exposure in Run 109. Conversion factor: 1 atm = 1.013×10^5 Pa.

30

Gas Side

Fe

S

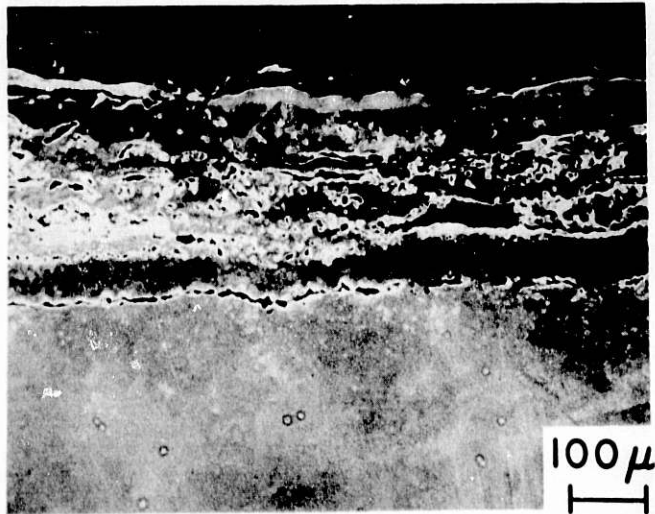Air Side

Run 104   Carbon Steel   Gas Temperature 1085 K $p_{O_2} = 2.7 \times 10^{-8}$ atm
                           Metal Temperature 977 K $p_{S_2} = 1.0 \times 10^{-17}$ atm

Fig. 24.   SEM Micrographs and Elemental Scans of Carbon Steel after a 500-h
            Exposure in Run 104.   Conversion factor: 1 atm = 1.013×10^5 Pa.
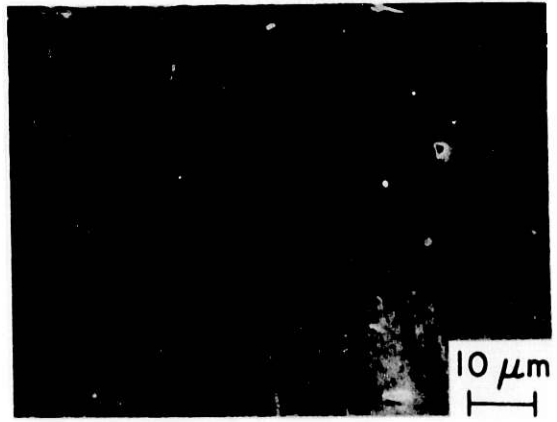
Gas Side

Air Side

Run 104
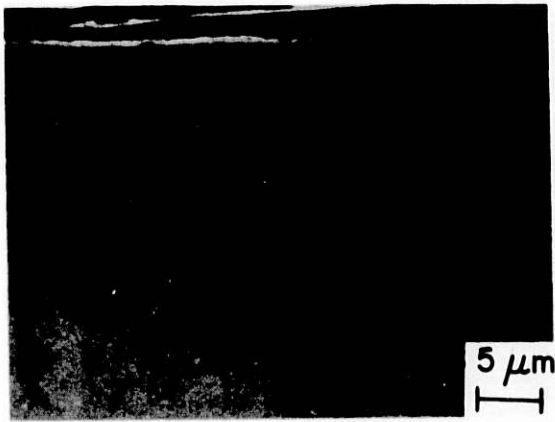
Fe- 2 1/4 Cr- 1 Mo

Gas Temperature 1085 K
Metal Temperature 977 K

$p_{O_2} = 2.7 \times 10^{-8}$ atm

$p_{S_2} = 1.0 \times 10^{-17}$ atm

Fig. 25. SEM Micrographs of Fe-2¼Cr-1Mo Steel After a 500-h Exposure in Run 104. Conversion factor: 1 atm = 1.013×10^5 Pa.

Gas Side
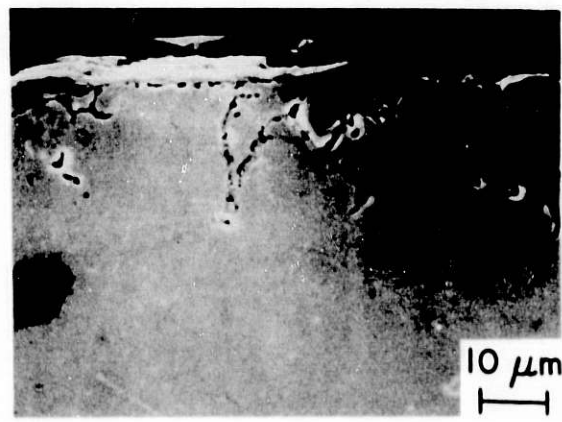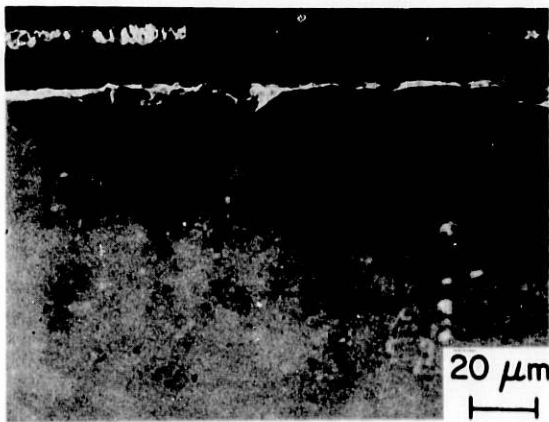
Air Side

Fe- 9 Cr- 1 Mo   Type 310 ss

Run 104   Gas Temperature 1085 K $p_{O_2} = 2.7 \times 10^{-8}$ atm
           Metal Temperature 977 K $p_{S_2} = 1.0 \times 10^{-17}$ atm

Fig. 26.   SEM Micrographs of Fe-9Cr-1Mo Steel and Type 310 Stainless Steel
            after a 500-h Exposure in Run 104.   Conversion factor: 1 atm =
            1.013×10^5 Pa.
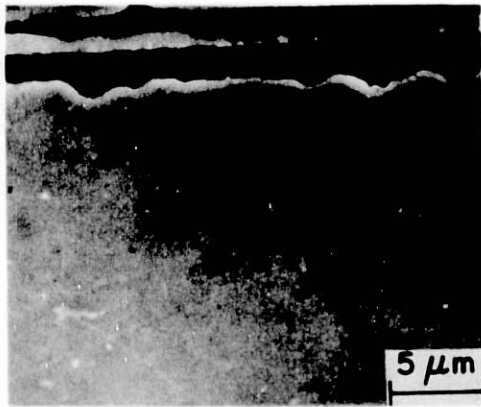
Gas Side

Air Side
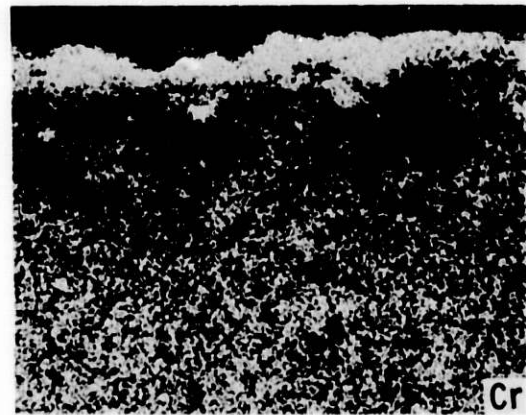
Run 104   Incoloy 800   Gas Temperature 1085 K
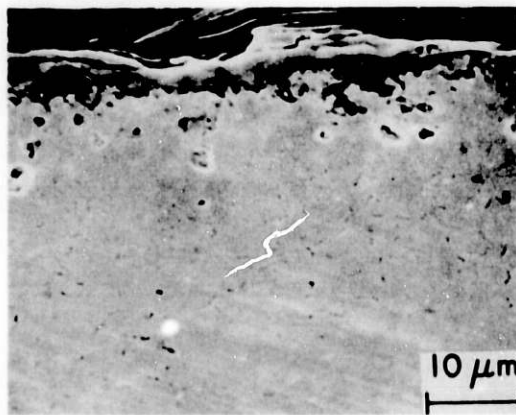   Metal Temperature 977 K

p_{O_2} = 2.7 x 10^{-8} atm

p_{S_2} = 1.0 x 10^{-17} atm

Fig. 27.   SEM Micrographs and Elemental Scans of Incoloy 800 after a 500-h
           Exposure in Run 104.   Conversion factor: 1 atm = 1.013 x 10^5 Pa.

34

Task D -- Erosion Behavior of Materials in Coal-conversion Processes
(J.Y. Park)

The objectives of the erosion program at ANL are to develop an engineering data base for the design of components subject to erosive wear in coal-conversion plants. Engineering design data will be obtained from erosion tests that will be performed at temperatures and in atmospheres designed to simulate actual plant conditions. The laboratory results will be compared with in-situ measurements currently being obtained from the NDT program at ANL.

In previous quarters, room-temperature erosion calibration tests were performed on 1015 carbon steel, Type 304 SS, Incoloy 800, Type 310 SS, and Stellite 6B using 150-μm Al_2O_3 particles with an impact velocity of 22 m/s and impact angles of 6-81° in an air environment. The erosion rate (mass loss/ mass impacted) was calculated from weight loss, and results were presented in previous reports[2,8] (Table V). The rates were in the range of 0.03-0.09 mg/g.

Corrosion calibration tests were performed on 1015 carbon steel, Type 304 SS, Incoloy 800, Type 310 SS, and Stellite 6B in a simulated gasifier atmosphere (18 CO, 12 CO_2, 5 CH_4, 24 H_2, 39 H_2O, 1 NH_3, and 1 H_2S in vol %) at 816°C for 150 h. The equilibrium oxidation potential, sulfur potential, and carbon activity of this atmosphere are calculated to be 5.4 x 10^{-19}, 3.5 x 10^{-7}, and 0.0214, respectively. Significant amounts of corrosion occurred in all specimens. Material degradation due to corrosion was measured in terms of weight change, loss of substrate thickness, scale formation, and internal corrosion. The results were presented in previous reports[3,9] and are summarized in Table VI. Carbon steel showed the greatest weight change, substrate loss, and scale formation. The corrosion scale of the carbon steel specimens contained many cracks. Cracks were also observed at the interface between the scale and the metal substrate; these may result in the exfoliation of the scale and influence the long-term corrosion-rate measurement. Internal corrosion was not apparent in the carbon steel, but occurred in the other alloys under the scale near the substrate surface.

Erosion-corrosion calibration tests were performed on 1015 carbon steel, Type 304 SS, Incoloy 800, Type 310 SS, and Stellite 6B using 150-μm Al_2O_3 particles with an impact velocity of 22 m/s and impact angles of 16-81° in the same simulated gasifier environment. Weight change (mass loss/mass impacted) of the specimens was reported previously[4] (Table VII). A pseudo-erosion rate which assumes no synergistic interaction between erosion and corrosion processes was calculated by subtacting equivalent weight change due to corrosion (Table VI) from total weight loss, and the results are presented in Table VIII. The pseudo-erosion rate may be an underestimate, since a synergistic interaction between erosion and corrosion processes may well exist.

During the present quarter, room-temperature erosion tests on 1015 carbon steel, Type 304 SS, Incoloy 800, Type 310 SS, and Stellite 6B were performed in the ANL low-temperature erosion test apparatus using 150-μm Al_2O_3 particles with an impact velocity of 22 m/s and impact angles of 16-81° in an air environment. The purpose of these tests is to confirm and verify the erosion calibration test results from the high-temperature erosion-corrosion test apparatus. The erosion rate (mass loss/mass impacted) was calculated

from weight-loss measurements (Table IX). The erosion rate ranges from 0.01- to 0.08 mg/g, and is in good agreement with the erosion rate obtained from the high-temperature erosion-corrosion test apparatus. The erosion rate as a function of impingement angle is plotted as shown in Figs. 28-32. The erosion rate is found to be higher at low impingement angles than at high angles. This is consistent with Finnie's model of erosion for ductile materials.[10]

TABLE V. Weight Changes (mg/g) Observed in Room-temperature Erosion Tests[a]

Material	Impingement Angle				
	6°	16°	26°	36°	81°
1015 Carbon Steel	0.09	0.05	0.05	0.03	0.02
Type 304 SS	0.06	0.04	0.04	0.03	0.02
Incoloy 800	0.06	0.06	0.04	0.04	0.03
Type 310 SS	0.03	0.05	0.04	0.03	0.03
Stellite 6B	0.06	0.05	0.04	0.03	0.03

[a]Air atmosphere; 150-μm Al_2O_3 at 22 m/s.

TABLE VI. Results of 816°C Corrosion Tests[a]

Material	150-h Tests				24-h Tests
	Weight Change, mg/mm^2	Substrate Thickness Change, mm	Scale Thickness, mm	Penetration, mm	Weight Change, mg/mm^2
1015 Carbon Steel	+2.12	−1.02	1.041	0.000	+0.113
Type 304 SS	+0.14	−0.08	0.058	0.089	+0.002
Incoloy 800	+0.31	−0.05	0.003	0.020	+0.003
Type 310 SS					+0.002
Stellite 6B	+0.05	−0.25	0.005	0.076	+0.003

[a]Simulated gasifier atmosphere.

TABLE VII. Weight Changes (mg/g) Observed in 816°C Erosion-Corrosion Tests[a]

Material	Impingement Angle				
	6°	16°	26°	36°	81°
1015 Carbon Steel	-	-0.03	-0.01	-0.01	+0.00
Type 304 SS	-	-0.09	-0.06	-0.06	-0.06
Incoloy 800	-	-0.07	-0.07	-0.07	-0.09
Type 310 SS	-	-0.06	-0.07	-0.07	-0.10
Stellite 6B	-	-0.08	-0.07	-0.06	-0.08

[a]Simulated gasifier atmosphere; 150-μm Al_2O_3 at 22 m/s.

TABLE VIII. Pseudo-erosion Rates (mg/g) Calculated from Data of Tables VI and VII

Material	Impingement Angle			
	16°	26°	36°	81°
1015 Carbon Steel	-36.53	-36.51	-36.51	-36.50
Type 304 SS	- 0.79	- 0.76	- 0.76	- 0.76
Incoloy 800	- 0.97	- 0.97	- 0.97	- 0.99
Type 310 SS	- 0.86	- 0.87	- 0.87	- 0.90
Stellite 6B	- 0.98	- 0.97	- 0.96	- 0.98

TABLE IX. Weight Changes (mg/g) Observed in Room-temperature Erosion Tests[a] Performed with ANL Low-temperature Test Apparatus

Material	Impingement Angle			
	16°	26°	36°	81°
1015 Carbon Steel	0.03	0.02	0.02	0.01
Type 304 SS	0.04	0.03	0.03	0.02
Incoloy 800	0.03	0.03	0.03	0.02
Type 310 SS	0.04	0.03	0.03	0.02
Stellite 6B	0.07	0.08	0.03	0.02

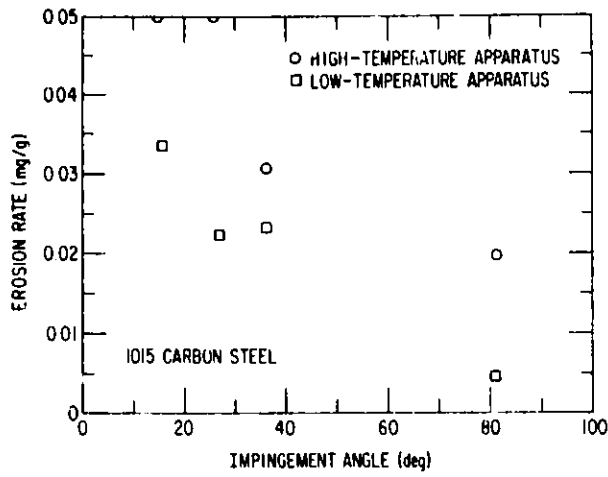[a]Air atmosphere; 150-μm Al_2O_3 at 22 m/s.

Fig. 28.   Erosion Rate vs Impinge-
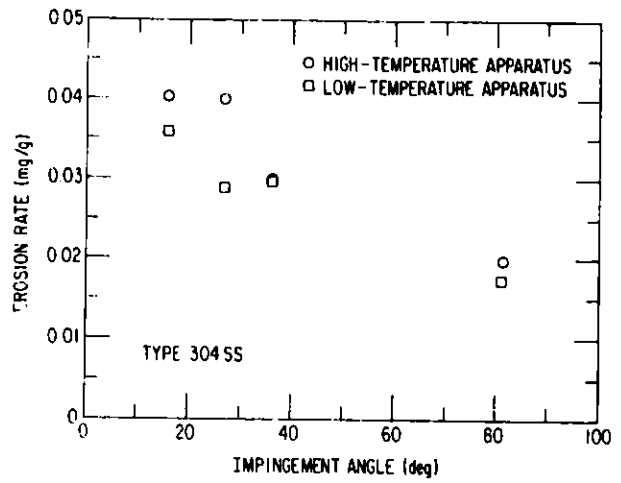ment Angle for 1015 Carbon Steel.

Fig. 29.   Erosion Rate vs Impingement
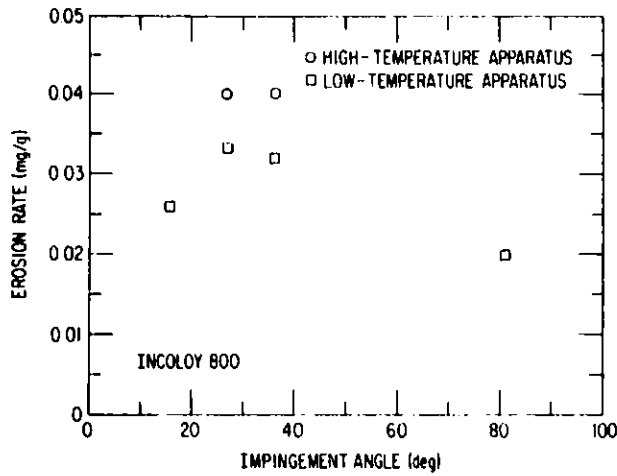Angle for Type 304 Stainless Steel.

Fig. 30.   Erosion Rate vs Impinge-
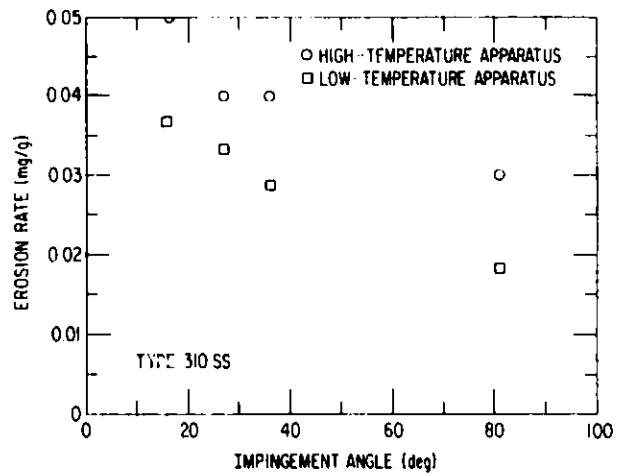ment Angle for Incoloy 800.

Fig. 31.   Erosion Rate vs Impingement
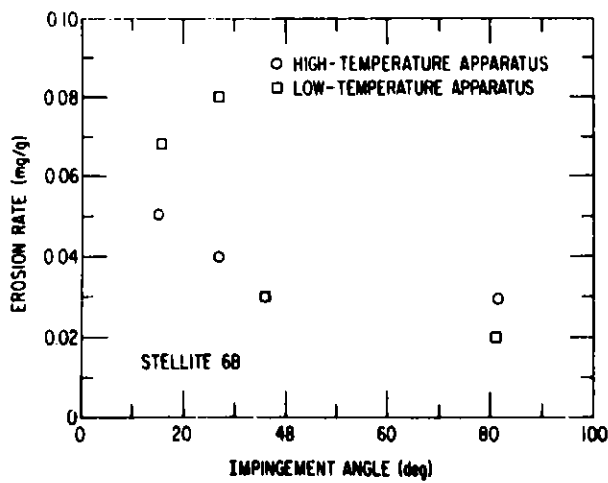Angle for Type 310 Stainless Steel.

Fig. 32.   Erosion Rate vs Impingement
Angle for Stellite 6B.

Task E — Failure Analysis *(D.R. Diercks and G.M. Dragel)*

1. Experimental Thermowells for IGT Ash Agglomerating (U-Gas) Gasifier

Seven experimental thermowells have been prepared for trial exposure
in the IGT Ash Agglomerating Gasifier (U-Gas) Pilot Plant, as described in a
previous report.[8] The lower portions of these thermowells are subject to
corrosive and erosive attack in service; the alloys and coatings used to
fabricate the lower portions of the experimental thermowells are given in
Table X. For the first series of exposures, thermowells 2, 3, and 7 were in-
stalled at positions approximately 1.1, 1.4, and 2.3 m (3.5, 4.5, and 7.5 ft),
respectively, above the normal operating height of the bed. Thermowell 1,
which is an uncoated Haynes 188 thermowell identical to thermowell 2, was
installed at a somewhat more erosive location approximately 0.4 m (1.4 ft)
above the top of the bed.

A total of six plant runs, each approximately four to five days
long, have been completed with the first four experimental thermowells in
place. The first three of these runs were made using relatively high-sulfur
Pittsburgh-seam coal; the fourth run used a mixture of Kentucky nos. 9 and 11
coals, and the fifth and sixth runs used washed Kentucky no. 9 coal. The bed
operating temperature for all six runs was typically in the range from 1024 to
1066°C (1875 to 1950°F).

An examination of the four experimental thermowells after the com-
pletion of the sixth run revealed significant degradition of thermowells 1
and 3; the condition of thermowells 2 and 7 cannot be determined without
removal. Therefore, these four thermowells will be removed and the remaining
three will be installed, with thermowell 5 in the position formerly occupied
by thermowell 2, thermowell 6 in the former thermowell 3 position, and thermo-
well 4 in the former thermowell 7 position. A detailed laboratory analysis of
the condition of the first four thermowells will be initiated after their
removal.

2. Hot-gas Sampler Coupling from IGT HYGAS® Pilot Plant

The analysis of a failed hot-gas sampler coupling from the IGT
HYGAS® Pilot Plant has been completed, and a final report is being prepared.
The coupling was part of a hot-gas sampling line used to withdraw batch-gas
samples from the steam-oxygen gasifier (SOG) zone of the plant on a continuous
basis. The coupling joined a 1.27-cm (0.5-in.)-OD line to a 1.91-cm (0.75-
in.)-OD line, and was located outside the reactor vessel at a point about 60
cm (2 ft) from the vessel wall. The failed component was made of RA 330, and
Inconel 182 weld metal was used to join it to the lines at either end.
Failure due to circumferential through-wall cracking occurred after 8470 h of
operation.

Visual and metallographic examinations of the failed coupling re-
vealed numerous circumferential and axial cracks. Most of the cracks
apparently initiated at the inner surface, and all were intergranular in
nature, with extensive branching commonly observed. Considerable interdendritic
cracking in the Inconel 182 weld filler metal was also seen.

In addition to the intergranular cracking, a gray corrosion product was observed in some of the grain-boundary regions of the base metal, particularly near the inner surface. Selected regions were examined by SEM-EDX, and some of the results obtained are presented in Fig. 33. The grain-boundary regions exhibit a very high sulfur content; both CrS and Ni₂S₃ phases appear to be present. Similar results were obtained from an examination of the Inconel 182 weld metal, except that the corrosive attack and cracking occurred in the interdendritic regions, and the Ni_3S_2 phase appeared to predominate.

The present failure is similar in several respects to the failure of an internal solids transfer line from the HYGAS Pilot Plant.[2,8,11] In the latter case, failure occurred by severe sulfidation attack of the high-Ni Inconel 182 weld metal. The resulting formation of Ni_3S_2, which formed a liquid eutectic with nickel at the operating temperature of the line, led to the attack of the adjacent Incoloy 800 and RA 330 base metal. The same sequence of events appears to have occurred in the present failure; the Inconel 182 weld metal was first attacked by the high-sulfur gaseous environment present in the coupling, and the resultant Ni_3S_2 formation caused subsequent intergranular attack and cracking of the adjacent base metal. The possible use of a lower-nickel weld filler metal or continuous water cooling of the coupling (the failed coupling appeared to have been intermittently water-cooled) was recommended to avoid future failures of the coupling.

3. Product Gas Line from Bi-Gas Pilot Plant

A failed 20.3-cm (8-in.)-OD product gas line from the Bi-Gas Coal-gasification Pilot Plant is presently being analyzed. The Schedule 140 line is made of Type 304 stainless steel, and the failure consisted of a circumferential crack extending approximately 270° around the pipe in the vicinity of a weld to an adjoining tee. Water, presumably due to condensation, was found inside the failed pipe when it was disassembled; the water had a pH of 8.5 and a chloride content of 4.5 ppm.

Initial metallographic results indicate the cracking present in the pipe to be intergranular and highly branched (Fig. 34). A simple qualitative procedure (ASTM Procedure A262, Practice A)[12] was used to determine the extent to which the piping material was sensitized; a moderate degree of grain-boundary sensitization was revealed. The intergranular nature of the cracking and the relatively low level of chlorides found in the condensate tend to rule out chloride-assisted stress-corrosion cracking, and the possibililty that hydroxides or dissolved oxygen caused the cracking is presently being explored. Additional SEM and x-ray analysis work is planned.

4. Product Gas Line Expansion Joint from IGT U-Gas Pilot Plant

A Type 321 stainless steel expansion joint bellows assembly from the product gas line of the IGT U-Gas Pilot Plant failed owing to pitting from the inner surface after approximately 127 h of operation. The failed component was located downstream from the gasifier cyclones and two gas quenching systems, and typically operated at a temperature of about 260°C (500°F) and a pressure of 40 to 80 kPa (6 to 11.5 psig). Some entrained coal char and ash were present in the product gas stream passing through the expansion joint.

The bellows are of a laminated construction made up of six plies, each approximately 0.23 mm (9 mils) thick. A single perforation was detected through the outermost ply at the outer surface of the bellows, but very extensive pitting and corrosive attack was observed at the inner surface of the innermost ply (see Figs. 35 and 36). Many of these pits extended through several plies, and probably would have completely perforated the bellows with additional time in service. The inner surface of the bellows was also coated with coal char and corrosion products, and particularly heavy deposits were present in the most heavily pitted regions.

Chemical analyses were performed on two samples of deposits taken from the inner surface of the bellows at a heavily pitted region. The chloride contents of these two samples were found to be 0.48 and 0.34 wt %, and the corresponding sulfate contents were 0.22 and 0.74 wt %, respectively. It should be noted that these values were probably influenced by a soap-and-water cleaning procedure that had inadvertently been used on the bellows assembly before sectioning and examination. Nonetheless, the failure probably resulted from chloride-induced pitting, with the necessary moisture produced by the condensation that occurred during shutdown. Tentative recommendations include heat-tracing the bellows assembly to avoid condensation during shutdown or using a more pitting-resistant material, possibly titanium, to fabricate the assembly. A final report on this failure will be prepared shortly.

TABLE X. Summary of Alloys and Coatings Used to Fabricate Lower Portions of Experimental Thermowells

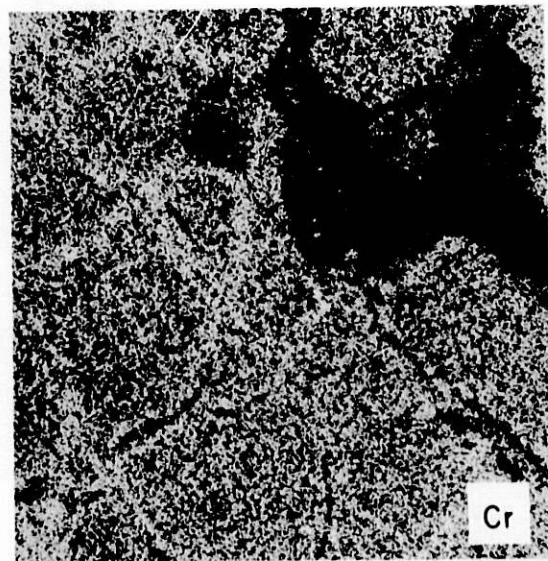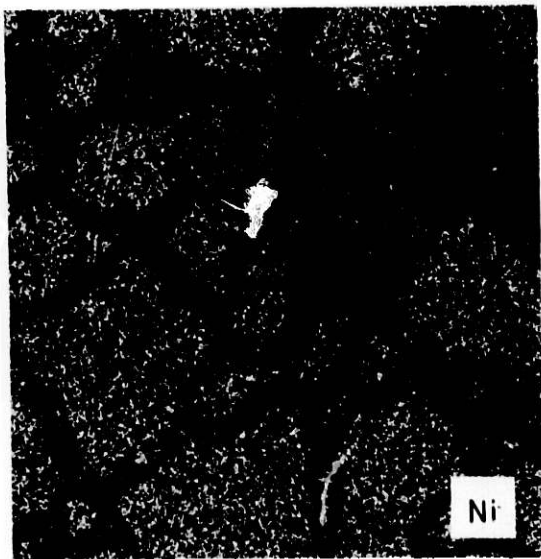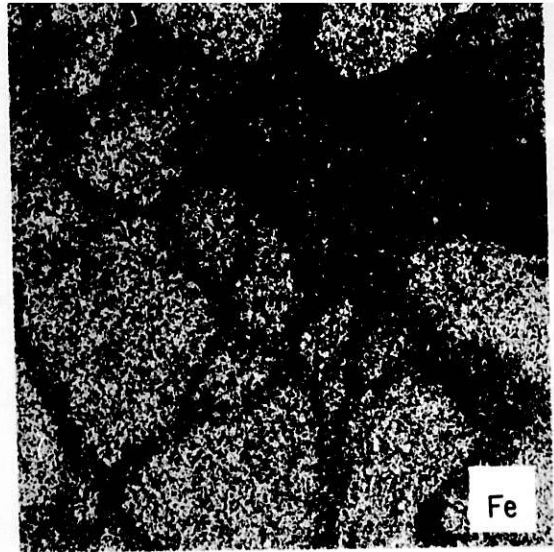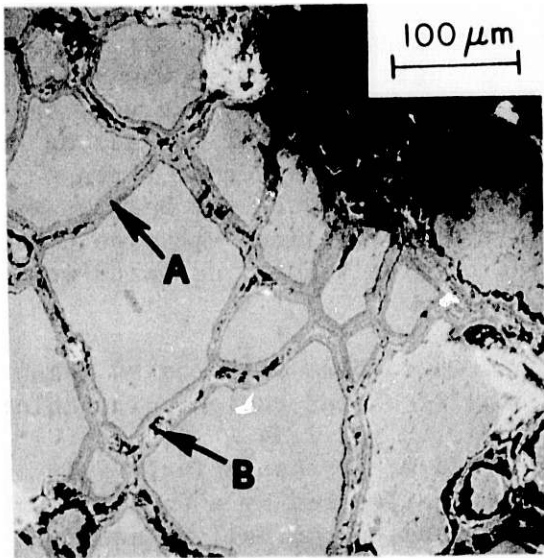| Thermowell No.	Alloy	Coating
1	Haynes 188	none
2	Haynes 188	none
3	Incoloy 800	Cr-Al-Hf
4	Incoloy 800	aluminized
5	Type 310 stainless steel	Cr-Si
6	Type 310 stainless steel	Cr-Al-Hf
7	Type 310 stainless steel	aluminized
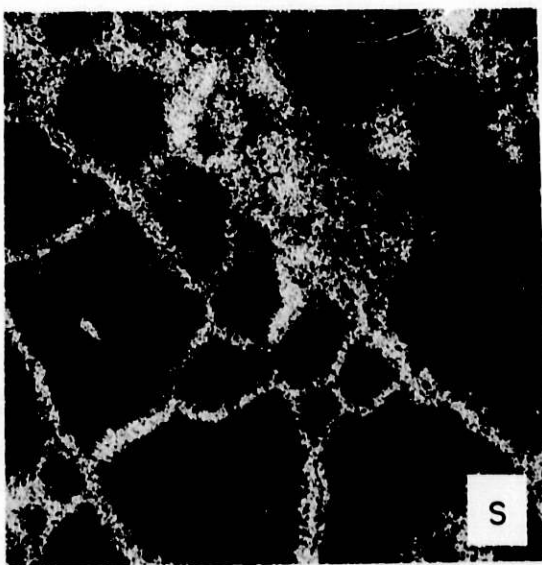
Fig. 33. SEM Micrograph and Elemental Scans of a Region of the Attacked Coupling near the Inner Surface.
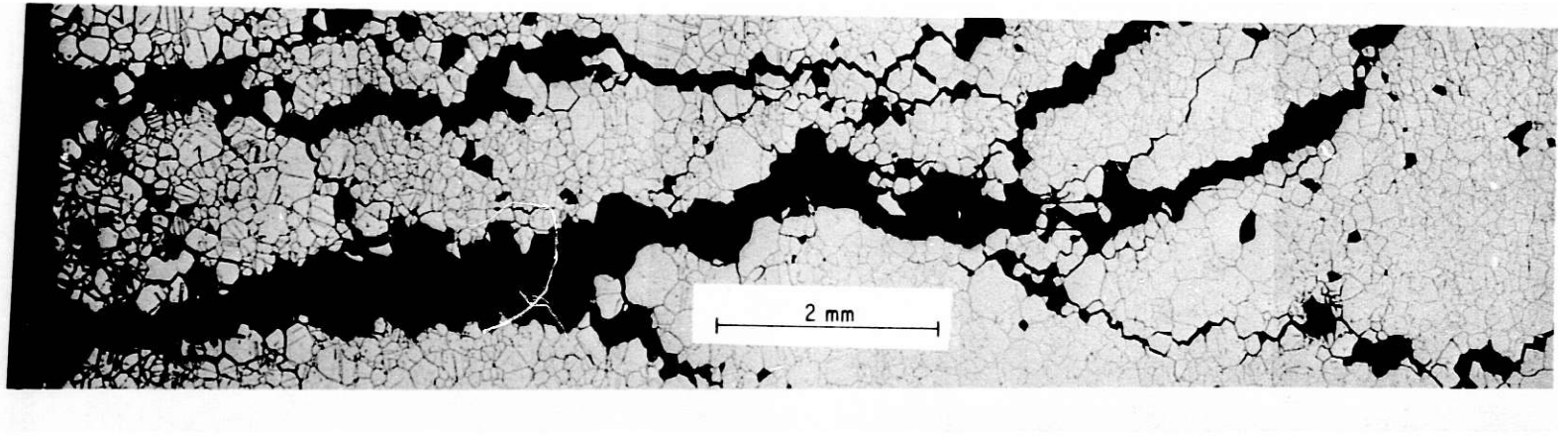
42

Fig. 34.   Cracking Present near Inner Surface of Bi-Gas Product Gas Line.
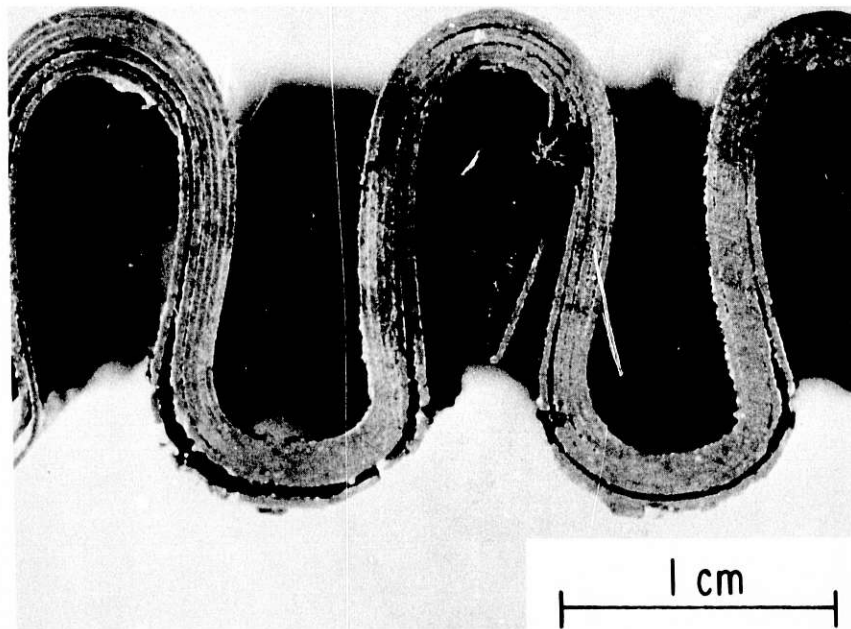
43

Fig. 35. Cross Section Through Failed Bellows from Product Gas Line
Expansion Joint in U-Gas Pilot Plant. The inner surface of the
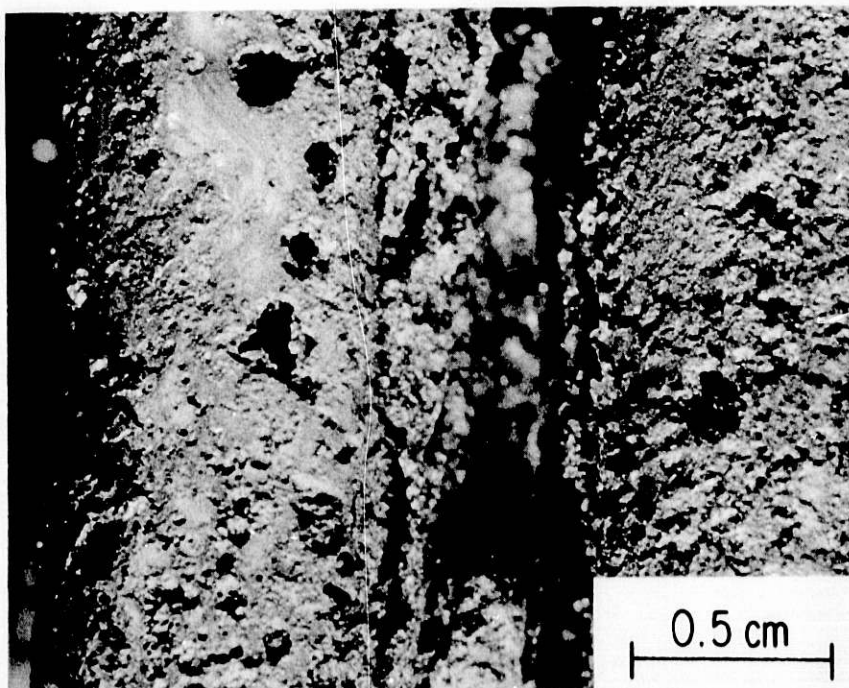bellows faces downward in the picture.

Fig. 36. Photograph of Inner Surface of Failed U-Gas Expansion Joint
Bellows, Showing Corrosive Attack and Pitting.

REFERENCES

1. R. Majkrzak, Grand Forks Energy Technology Center, Grand Forks, ND, personal communication.

2. W.A. Ellingson et al., Materials Technology for Coal-conversion Processes, Progress Report for April-June 1980, Argonne National Laboratory Report ANL-80-93, pp. 11-14.

3. W.A. Ellingson et al., Materials Technology for Coal-conversion Processes, Progress Report for July-December 1979, Argonne National Laboratory Report ANL-80-12, pp. 8-34.

4. Josef and Herbert Krautkramer, Ultrasonic Testing of Materials, 2nd Ed., Springer-Verlag, New York, p. 20 (1977).

5. L. Filipczynski, Z. Pawlowski, and J. Wehr, Ultrasonic Methods of Testing Materials, Butterworths, London, p. 6 (1966).

6. M. Kumugai, R. Uchimura, and H. Kishidaka, A Testing Method for Spalling Resistance of Refractories and Its Application to Q-BOP Refractories, Paper Summaries, National Fall Conference of the American Society for Nondestructive Testing, Houston, TX, October 6-9, 1980, pp. 19-27.

7. W.A. Ellingson et al., Materials Technology for Coal-conversion Processes, Seventeenth Quarterly Report, January-March 1979, Argonne National Laboratory Report ANL-79-56.

8. W.A. Ellingson, et al., Materials Technology for Coal-conversion Processes, Progress Report for January-March 1980, Argonne National Laboratory Report ANL-80-46, p. 24.

9. W.A. Ellingson et al., Materials Technology for Coal-conversion Processes, Eighteenth Quarterly Report, April-June 1979, Argonne National Laboratory Report ANL-79-93, pp. 1-10.

10. I. Finnie, Erosion by Solid Particles in a Fluid Stream, Symp. on Erosion and Cavitation, ASTM STP 307, pp. 70-82 (1962).

11. D.R. Diercks, Analysis of Failed Transfer Line from the IGT HYGAS Coal Gasification Pilot Plant, to be presented at the Symposium on Material-Environment Interactions in Structural and Pressure Containment Service, 1980 ASME Winter Annual Meeting, Chicago, IL, November 16-21, 1980.

12. Detecting Susceptibility to Intergranular Attack in Stainless Steels, Standard A262, Practice A, Annual Book of ASTM Standards, Part 3, American Society for Testing and Materials, Philadelphia (1974).